

**CONNECTIVITY AND DISCONNECTIVITY: A
MULTIMODAL APPROACH TO
UNDERSTANDING AND PREDICTING MOTOR
RECOVERY**

A Dissertation

Presented to the Faculty of the Weill Cornell

Graduate School of Medical Sciences

in Partial Fulfillment of the Requirements for the Degree of

Doctor of Philosophy

by

Emily Olafson

May 2023

© 2023 Emily Olafson

ALL RIGHTS RESERVED

CONNECTIVITY AND DISCONNECTIVITY: A MULTIMODAL APPROACH
TO UNDERSTANDING AND PREDICTING MOTOR RECOVERY

Emily Olafson, Ph.D.

Cornell University 2023

Your abstract goes here. Make sure it sits inside the brackets. If not, your biosketch page may not be roman numeral iii, as required by the graduate school. The abstract should state the problem, describe the methods and procedures used, and give the main results or conclusions of the research. The abstract must not exceed 350 words in length (generally about one-and-one-half correctly spaced pages; the abstract may not be more than two pages).

BIOGRAPHICAL SKETCH

Emily was born in Northhampton, United Kingdom in 1997, and grew up in Toronto, Canada. In highschool, her interest in biology was nurtured by an exceptional biology teacher. In her first year at McGill University in Montreal, she was excited by the interdisciplinary nature of the Neuroscience major program, and ultimately joined the Honors stream where she would be able to pursue a full-year undergraduate thesis. In her second year, she worked in the lab of Dr. Artur Kania where she was able to apply cutting-edge technologies like CRISPR-Cas9 to modify the genome of chick embryos and analyze changes in spinal cord formation.

Wanting to explore computational neuroscience, she reached out to Mallar Chakravarty and joined his lab at the Douglas Mental Health University Institute processing T1w scans from individuals with autism spectrum disorder through MAGeT-Brain, a subcortical segmentation algorithm. Her interest in human neuroimaging skyrocketed after she took a master's course in neuroimaging taught by Mallar. This course taught her how to critically engage with literature, how to articulate complex ideas, and ultimately pushed her to apply to graduate school.

She applied to neuroscience programs across the US and ultimately ended up at Weill Cornell Graduate School in New York City. She rotated with Amy Kuceyeski, exploring the relationship between structural and functional connectivity after stroke, and with Sudhin Shah, investigating neural correlates of consciousness in a minimally conscious patient. Although COVID prevented her from rotating with other labs, she had already decided on joining Amy's lab, and moved to Ithaca in August 2020.

In Amy Kuceyeski's lab, she did a variety of things.

She taught 2 semesters in the Cornell Prison Education Program: first at Five Points Correctional Facility, and then at Cayuga Correctional Facility. She generated material for the course "Neurochemistry of Human Behavior" and taught incarcerated people about synaptic transmission, long term potentiation, and mechanisms of disease.

She did an internship at Biogen in their clinical imaging group.

To my parents, I dedicate this dissertation with my deepest gratitude.

ACKNOWLEDGEMENTS

Thank you to Amy Kuceyeski, my mentor at Weill. Aside from your scientific brilliance, your compassionate and trusting leadership was invaluable to me throughout my thesis, but especially during the pandemic. You consciously create an environment in which people can thrive. You rock. I am deeply appreciative of my thesis committee: Dr. Conor Liston, Dr. Nicholas Schiff, and Dr. Aaron Boes, for their support and expertise, both academically and professionally.

I would also like to thank the people who made Ithaca feel like home: Parker Singleton, Ceren Tozlu, Keith Jamison, Zijin Gu, Ben, and Liam.

Thank you to mentors along the way: Mallar Chakravarty, Elvisha Dhamala, Gabriel Devenyi, Saashi Bedford, Raihaan Patel, Elisa Guma, Artur Kania, Daniel Morales, Sylvie Lahaie, Alyssa Dai, Jonathan DuBois, and Cindy Law.

To others who have made difficult experiences easier: Clive Liew, Mert Sabuncu, Randi Silver, Rebekah Ciribassi, thank you.

Thank you to my world-class friends who remind me that people are fundamentally good: Emma, Miriam, Mikey, Zoe, Nilasha, Jonah, CEC, Jasmine, Max, Board Games Club, and my Neuro entire cohort.

To the students and staff of the Cornell Prison Education Program: teaching at Five Points and Cayuga was the best thing I've ever done. From the bottom of my heart, thank you for the opportunity.

To my parents, thank you for the sacrifices you've made to give me a stellar education. Thank you to my twin brother Matt, for being a lifelong best friend.

Finally, one last thank you is reserved for my partner, Isaac, for answering all my statistics questions, for eating expensive sushi with me, and for generally being the light of my life.

TABLE OF CONTENTS

Biographical Sketch	iii
Dedication	v
Acknowledgements	vi
Table of Contents	vii
List of Tables	ix
List of Figures	x
1 Functional connectome reorganization relates to post-stroke motor recovery and structural and functional disconnection*	1
1.1 Introduction	1
1.2 Methods	4
1.2.1 Data description	4
1.2.2 Structural data processing	6
1.2.3 Functional data processing	6
1.2.4 Functional connectivity calculation	7
1.2.5 Estimated structural disconnection	9
1.2.6 Estimated functional disconnection	12
1.2.7 Graph matching	12
1.2.8 Quantification of functional reorganization	13
1.2.9 Statistical analyses	15
1.2.10 Code availability	17
1.3 Results	17
1.3.1 Functional reorganization is primarily observed in the brainstem and cerebellum	17
1.3.2 Regions with greater structural and functional disconnection have more functional reorganization over time	24
1.3.3 Functional reorganization is related to impairment and recovery	32
1.3.4 Robustness of results	37
1.4 Discussion	37
1.4.1 Limitations	42
1.5 Conclusion	43
2 Frontoparietal network activation is associated with motor recovery in ischemic stroke patients*	44
2.1 Introduction	44
2.2 Methods	48
2.3 Results	59
2.4 Discussion	59
2.5 Conclusions	59

3	Chapter 3	60
3.1	Introduction	60
3.2	Methods	64
3.2.1	Sample demographics	64
3.2.2	General overview	68
3.2.3	Description of models and their inputs	70
A	Supplementary material for Chapter 1	77

LIST OF TABLES

LIST OF FIGURES

1.1	Overview of individuals' stroke lesions, resulting structural disconnection and Fugl-Meyer score trajectories.	5
1.2	Overview of the graph matching procedure.	10
1.3	Visualization of node-level remapping frequencies and group-level structural connectivity disruptions due to the lesion.	19
1.4	Relationships between FC disruption, SC disruption, and remapping over the 1 week - 2 week time interval post-stroke.	26
1.5	Relationship between subject-level remapping, baseline motor impairment, eventual motor recovery.	33
2.1	Clustering of time series data and quantification of dynamic state metrics. a. Time series data from all subjects were concatenated together along the time dimension. K-means clustering produced 4 distinct brain activation states defined by different locations in regional activation space (image adapted from Cornblath et al. 2020). Each TR is assigned to one of four brain states based on k-means partitions. b. Fractional occupancy, dwell time, appearance rate, and transition probabilities are calculated separately for each subject and for each state.	47
3.1	Sensorimotor tract template atlas (SMATT), displaying only right hemisphere tracts relative to an MNI template. Includes supplementary motor area (SMA), dorsal premotor cortex (PMd), ventral premotor cortex (PMv), pre-supplementary motor area (pre-SMA), primary sensory cortex (S1), and primary motor cortex (M1). Pre-SMA is the most anterior tract, S1 is the most posterior tract.	71
3.2	Overview of the Network Modification tool. Binary lesion masks in MNI space representing the presence of a stroke lesion (turquoise) in a given voxel are provided by the user. Each lesion mask is embedded into 420 unrelated healthy structural connectomes (separately for each healthy subject) and the regional or pairwise change in connectivity (ChaCo) scores are calculated and averaged across healthy subjects (parcellation shown here is the Shen 268-region atlas).	72
A.1	Functional network visualizations.	77
A.2	Results of optimization procedure to choose the best regularization parameter, lambda (λ).	78
A.3	Functional connectivity (node strength) differences between stroke and control subjects.	79

CHAPTER 1

**FUNCTIONAL CONNECTOME REORGANIZATION RELATES TO
POST-STROKE MOTOR RECOVERY AND STRUCTURAL AND
FUNCTIONAL DISCONNECTION***

1.1 Introduction

Motor deficits are among the most common and disruptive symptoms of ischemic stroke. Spontaneous recovery of motor function occurs for most patients (Duncan, Lai, and Keighley 2000), and largely depends on the ability of brain networks to functionally reorganize and compensate for lost function (Grefkes et al. 2008; Rehme and Grefkes 2013). As demonstrated by animal models, the functionality of damaged motor regions may be remapped to surviving tissue around the lesion (Winship and Murphy 2009). However, brain areas distant to the lesion that have similar function and/or connectivity as the damaged area have also been shown to compensate for lost function (Winship and Murphy 2009; Adam et al. 2020; Murata et al. 2015; Brown et al. 2009).

In humans, functional reorganization has been studied with functional magnetic resonance imaging (fMRI). Task fMRI studies have demonstrated that cortical reorganization related to motor recovery can be characterized by task-based activation of surviving ipsilesional cortex, contralateral areas, and even regions

* Olafson, E. R., Jamison, K. W., Sweeney, E. M., Liu, H., Wang, D., Bruss, J. E., Boes, A. D., and Kuceyeski, A. (2021). Functional connectome reorganization relates to post-stroke motor recovery and structural and functional disconnection. *NeuroImage*, 245, 118642.

not classically activated by motor tasks in healthy subjects (Ward et al. 2003). Recently, resting-state fMRI has emerged as a means to study connectivity changes after stroke in subjects who are severely impaired and cannot perform motor tasks. Resting-state fMRI has been used to identify recovery-related changes in functional connectivity between specific brain regions, reflecting network-level changes (Park et al. 2011). However, few studies to date have attempted to capture longitudinal network-level reorganization after stroke using resting-state fMRI.

Prior studies investigating neural correlates of motor recovery have also focused almost exclusively on supratentorial strokes that impact the internal capsule and surrounding areas. Infratentorial pontine strokes may impact the corticospinal tract directly or the connections between motor cortex and the cerebellum (Lu et al. 2011). These strokes account for roughly 7 percent of all ischemic strokes (Saia and Pantoni 2009), and may have different mechanisms of recovery-related reorganization from those of more well-studied supratentorial strokes.

Remote brain areas anatomically connected to the lesion undergo structural and functional changes through a process known as diaschisis (Carrera and Tononi 2014). Functional remapping of areas structurally disconnected by the lesion may be an important component of the recovery process that has not been deeply explored. Recent studies have also demonstrated that functional connectivity (FC) changes occur following structural connectivity disruption after stroke (Lu et al. 2011; Griffis et al. 2020). We hypothesize that functional reorganization may also occur in areas whose FC is reduced due to the stroke. In this study, we propose a novel measure to capture adaptive functional network

reorganization after pontine stroke, outlined below, and relate it to patterns of regional stroke-related structural connectome disruption and measures of upper-arm motor recovery.

Connectivity to the rest of the brain is one aspect of a brain region's functional role in the network. We propose that instances of functional reorganization over time may be captured by identifying brain regions whose pattern of FC with the rest of the brain is more closely matched by a different brain region at a later date. Considering functional connectomes as a graph, the task of identifying similar nodes (gray matter regions, in this case) between two functional connectomes can be considered a graph matching problem (Conte et al. 2004). Conceptually, the process of graph matching exchanges the labels of regions in a network when doing so results in increased similarity of the two networks. When two regions exchange FC profiles, the regions are said to have been 'remapped'. We hypothesize that graph matching, applied recently to brain networks for the first time to assess the relationship between functional and structural connectivity networks (Osmanlıoğlu et al. 2019), will allow accurate quantification of whole brain, network-level, recovery-relevant functional reorganization after stroke.

As far as we know, no work has attempted to detect connectivity network-level functional reorganization in post-stroke recovery with longitudinal MRI, much less correlate it with measures of recovery or patterns of structural connectome damage. We hypothesize that 1) brain regions with more structural and functional damage due to the stroke will more frequently functionally reorganize, 2) more impaired subjects will have more early functional reorganization in the sub-acute stages, 3) the amount of early reorganization will be correlated with

long-term recovery, and 4) the amount of functional reorganization over time will correlate with the change in motor impairment between subsequent sessions.

1.2 Methods

1.2.1 Data description

The data consist of 23 first-episode stroke patients (34-74 years old; mean age 57 years; 8 female) with isolated pontine infarcts and 24 healthy age- and sex-matched controls (33-65 years old; mean age 52 years; 10 female). A subset of the data (11 stroke subjects and 11 healthy control subjects) used here has been previously described in Lu et al., 2011; this study includes an additional 12 stroke subjects and 13 control subjects. Of the twenty-three stroke subjects, fourteen had right brainstem infarcts and nine had left brainstem infarcts (Figure ??A). Patients were scanned five times over a period of 6 months. Specifically, MRIs were obtained at 7, 14, 30, 90 and 180 days after stroke onset on a 3T TimTrio Siemens using a 12-channel phase-array head coil. Fugl-Meyer motor scores were obtained twice at each session, and later averaged and normalized to a range of 0-100 (Figure ??B). Anatomical images were acquired using a sagittal MP-RAGE three-dimensional T1-weighted sequence (TR, 1600ms; TE 2.15ms; flip angle, 9°, 1.0 mm isotropic voxels, FOV 256 x 256). Each MRI session involved between two and four runs of resting-state fMRI at 6 minutes each. Subjects were instructed to stay awake with their eyes open; no other task instruction was provided. Images were acquired using the gradient-echo echo-planar pulse sequence (TR, 3000ms; TE, 30ms; flip angle, 90°, 3 mm isotropic voxels).

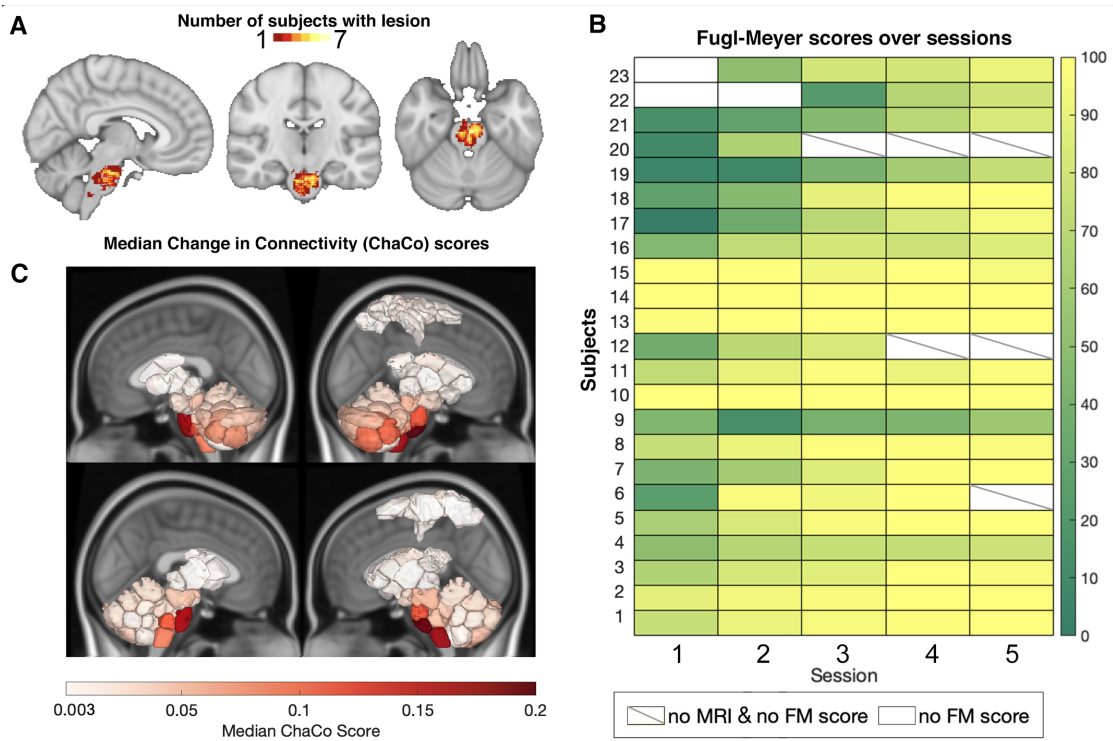


Figure 1.1: Overview of individuals' stroke lesions, resulting structural disconnection and Fugl-Meyer score trajectories.

A. Distribution of lesions across the brain. Colors indicate the number of subjects with a lesion in that voxel. **B.** Normalized Fugl-Meyer scores for all subjects over the five post-stroke sessions. Boxes colored white indicate missing motor scores and diagonal lines within the box indicate missing MRI data for the corresponding time point. **C.** Group median structural disconnection scores for each brain region calculated as the number of streamlines connected to each region that intersect with the lesion, normalized by the total number of streamlines connecting to that region (only displaying regions with ChaCo scores > 0.003 corresponding approximately to $\log(\text{ChaCo}) < -6$). Cortical areas with non-zero median ChaCo scores reflect motor regions at the end of disrupted corticospinal tracts. Top row of each subject inset shows a lateral view of the brain, bottom row of each inset shows a medial view.

1.2.2 Structural data processing

Preprocessing of the longitudinal structural data included affine registration of each subject's T1 scans to the baseline T1 scan, collapsing co-registered files to an average T1 and creation of a skull-stripped brain mask followed by manual editing and binarization of the hand-edited mask. The brain mask was then transformed back to each of the follow-up T1s in native space using the inverse registration acquired from the first step. This was followed by bias field correction of all the T1 scans, transformation of native-space bias field-corrected data back to baseline space, and the creation of an average bias field-corrected scan for each subject. Stroke lesion masks were hand-drawn on these transformed T1 scans by ADB and JEB. Structural normalization was performed with the CONN toolbox (Whitfield-Gabrieli and Nieto-Castanon 2012).

1.2.3 Functional data processing

Preprocessing of the longitudinal functional data was performed using the CONN toolbox (Whitfield-Gabrieli and Nieto-Castanon 2012), including functional realignment of volumes to the baseline volume, slice timing correction for alternating acquisition, segmentation and normalization, and smoothing with a 4mm FWHM kernel. The WM and CSF probability maps used to derive WM and CSF BOLD signal were first thresholded above 50% for each subject, and a one-voxel binary erosion step was applied to these thresholded maps (Whitfield-Gabrieli and Nieto-Castanon 2012). This was followed by a denoising protocol (CompCor) (Behzadi et al. 2007) which regressed out the cerebrospinal fluid and white matter signal, as well as 24 realignment parameters (added

first-order derivatives and quadratic effects). Temporal band pass filtering (0.008 - 0.09Hz), despiking and global signal removal regression were also performed. The first four frames of each BOLD run were removed. Frame censoring was applied to scans with a framewise displacement threshold of 0.5 mm along with its preceding scan (Power et al. 2012a). Regional time series were acquired by parcellating the scans into 268 non-overlapping brain regions using a functional atlas derived from healthy controls (Shen et al. 2013) and averaging the time course of all voxels within a given region. Voxels identified as lesioned were excluded from regional timeseries calculations. Regions were assigned to one of 8 functional networks (Figure S1), identified by (Finn et al. 2015) using spectral clustering in healthy subjects.

1.2.4 Functional connectivity calculation

Functional connectivity (FC) matrices were calculated as the regularized inverse of correlation matrices. Calculating FC using precision minimizes the effect of indirect connections and has been shown to result in connectomes that are more similar to structural connectivity (Wodeyar et al. 2020; Liégeois et al. 2020). To compute the precision FC, we first calculated the full Pearson correlation-based FC (Σ_i) for each individual i by correlating region-pair time series. We then took the unregularized inverse of Σ_i , denoted P_i , and averaged them over the i subjects to obtain the population-level precision FC matrix P_{avg} . We then calculated the individual precision FC matrices using Tikhonov regularization, which adds a full-rank regularization term (scaled identity) to the correlation matrix before inversion (Liégeois et al. 2020).

$$P_i^{reg} = (\Sigma_i + \lambda \cdot I)^{-1}$$

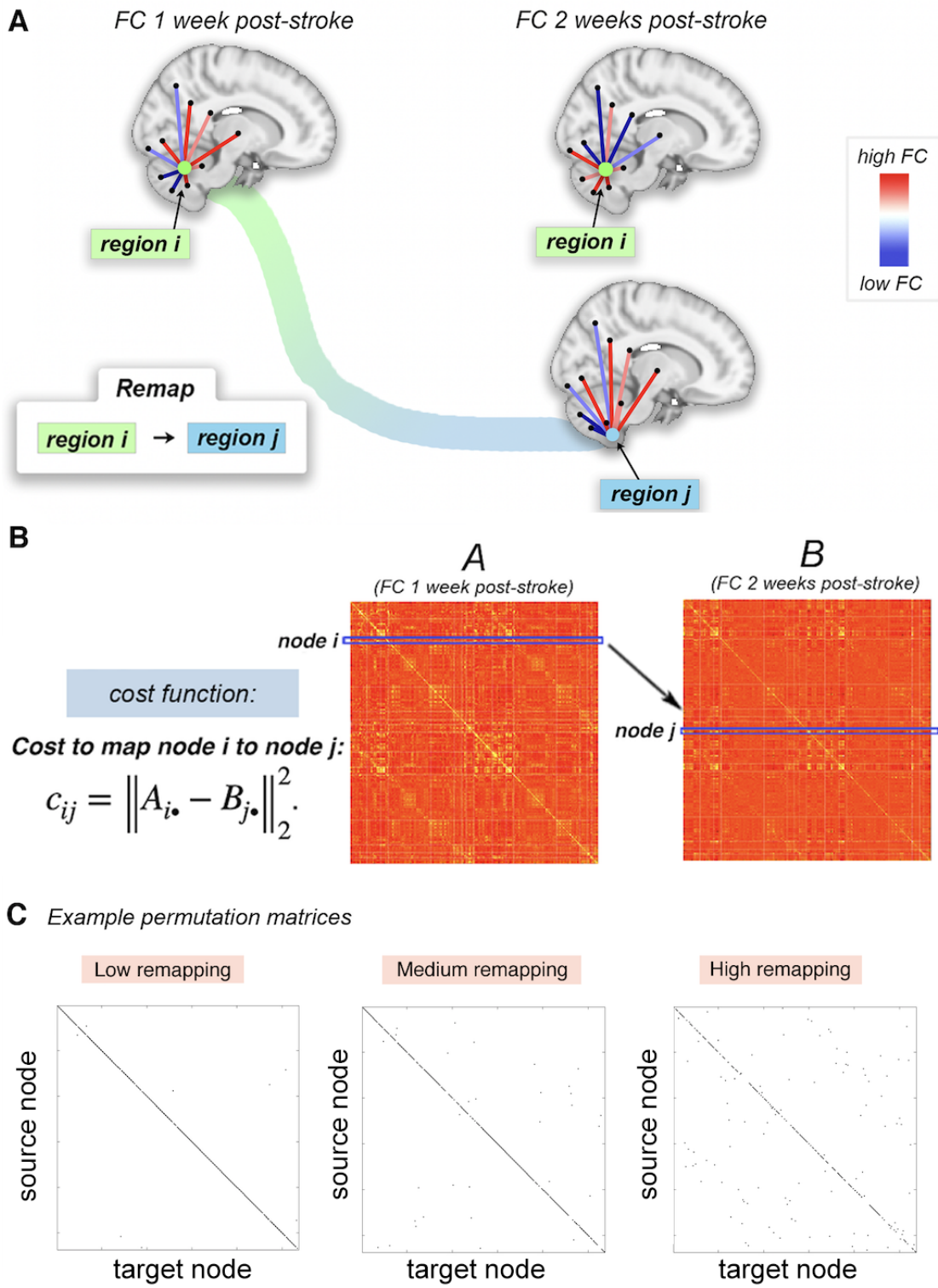
where I is the identity matrix and $\lambda \in [0, 1]$ is the regularization parameter. The regularization parameter λ was chosen via a grid search to be the value that minimized the root mean squared error of the Frobenius norm of the difference in regularized subject precision matrices P_i^{reg} and the population-level unregularized precision matrix P_{avg} , which was found to be $\lambda = 0.71$ (Figure S2). Partial correlation (precision) involves the inversion of the correlation matrix, and to stably invert this matrix, regularization is needed. Tikhonov regularization (a.k.a. L2 ridge regression), employed here, involves addition of an identity term scaled by a constant λ . The group average unregularized precision matrix is only used for the optimization of this λ term, not in the matrix inversion, and is performed as previously described (Liégeois et al. 2020; Golub, Hansen, and O’Leary 1999). The unregularized group average precision matrix is used as a benchmark for tuning this hyperparameter, as some of the inversion noise has been smoothed out in the calculation of the average. The values along the diagonal were set to 0 prior to graph matching; this is a form of regularization that penalizes off-diagonal swaps, which we employ to control the effect of regions with low SNR; a noisy region will be more likely to be assigned to itself because the zeroes are aligned. For completeness, the main analyses have been replicated with Pearson correlation-based FC, and results are provided in the supplementary material (Figure S13, S14, S15), with few differences to the overall findings with the precision FC.

1.2.5 Estimated structural disconnection

Deficits from subcortical stroke may be related to functional alterations at distant sites via metabolic diaschisis (Hillis et al. 2002; Corbetta et al. 2015) or remote degeneration that spreads along the white matter connectivity network (Duering et al. 2015; Cheng et al. 2015). In order to account for the impact of lesions on the structural connectome, the extent of regional structural connectivity (SC) disruption due to the lesion was assessed for each stroke subject with the Network Modification (NeMo) Tool (Kuceyeski et al. 2013). The NeMo Tool v2 requires only an individual's lesion mask in MNI space, which was obtained as described above, to produce an estimate of structural disconnection to each brain voxel, or to each region in a user-defined atlas. The newest version of the NeMo Tool, originally published in 2013, includes a reference database of SC from 420 unrelated individuals from the Human Connectome Project's (HCP) 1200 release (50 percent female, aged 25-35). The NeMo Tool begins by mapping the lesion mask into this healthy database's collection of tractography streamlines that quantify likely white matter pathways. It then identifies streamlines that pass through the lesion mask and records the gray matter voxels/regions that are at the ends of that streamline. The NeMo Tool produces the regional structural disconnection vector (ChaCo score, Change in Connectivity) that is an estimate of the percent of damaged streamlines at each voxel or region in the atlas. ChaCo scores were calculated for each stroke subject and the median was taken across the sample to create a group-level structural disconnection map (Figure 2.1C).

Figure 1.2: Overview of the graph matching procedure.

A. Example of a pair of regions that remap. Region i at 1 week post-stroke and region j at 2 weeks post-stroke have highly similar FC with the rest of the brain (moreso than region i at 1 week to region i at 2 weeks). The cost to remap i to j is low, and these regions would likely be remapped in the graph matching algorithm. **B.** The cost of remapping each region pair is used as input to the graph matching algorithm; the output of graph matching is the assignment of each region in one imaging session to a single corresponding region in the subsequent imaging session. If this assignment is to a different region, then it said to have "remapped". **C.** Three examples of permutation matrices of three subjects with varying amounts of remapping; black entries represent the assignment of a source node (y-axis) to its target node (x-axis).



1.2.6 Estimated functional disconnection

For each subject, we use FC matrices derived as described above to calculate the node strength, which quantifies the overall strength of all connections to and from a node, calculated the sum of all FC connection to the node (excluding a node's connection weight to itself). Then, for each time point, we performed an unpaired two-sided t-test at each node to determine whether its node strength was significantly different between stroke subjects and controls. The 268 p-values were corrected for multiple comparisons using Benjamini-Hochberg FDR correction at a corrected alpha of 0.05. We observed node strength disruptions in the stroke subjects at 1 week, 2 weeks, and 6 months post stroke, where stroke subjects had lower node strength in the brainstem, cerebellum, and temporal lobes compared to controls, and increased node strength in the lateral and medial frontal cortex (Figure S3).

1.2.7 Graph matching

We used a graph matching algorithm to capture FC network reorganization over time (Figure ??). Graph matching is an algorithmic process that maximizes the similarity between two networks by identifying an optimal mapping between nodes in the networks. One approach to identifying this optimal mapping is with a combinatorial optimization problem known as linear assignment.

Take two $n \times n$ networks A and B and a cost function $c : A \times B \rightarrow \mathbb{R}$ that determines the cost of assigning each node in A to each node in B . Entries in the cost matrix $C = (c_{ij})$ are defined by the Euclidean distance between row i in A and row j in B , i.e. $c_{ij}(A, B) = \|A_{i\bullet} - B_{j\bullet}\|_2^2$. In our application, the

rows $A_{i\bullet}$ and $B_{j\bullet}$ represent region i and region j 's FC to the rest of the brain, or FC profile, respectively. The linear assignment problem aims to construct the permutation matrix $P = (p_{ij})$ that minimizes the sum of the elements in cost matrix, i.e. $\min_P \sum_{i=1}^n \sum_{j=1}^n c_{ij} p_{ij}$. The matrix P is a permutation matrix with exactly one entry equal to 1 in each row and column, the rest being zero. Ones in the diagonal of P indicate the same node in the two networks were mapped to one another, while ones in the off-diagonal indicate a node was “remapped” to another node.

Here, we use the Hungarian algorithm to solve this minimization problem and find the corresponding optimal permutation matrix P . Figure ?? illustrates how the graph matching is applied to subsequent longitudinal FC networks in the same individual (either post-stroke or control) and depicts an instance of remapping in a single subject. In Figure ??A, the FC profile of brain region i (green region) at 1 week post-stroke is more closely matched by the FC profile of region j (blue region) at 2 weeks post-stroke than it is to itself at 2 weeks post-stroke. Example permutation matrices for three stroke subjects (one with high amount of remapping, one with an average amount of remapping and one with a low amount of remapping) are also provided.

1.2.8 Quantification of functional reorganization

We make assumption that remapping in the healthy controls is due to noise. Then, to remove this noise, we observed the set of nodes to which node x got assigned in the healthy control population along with their frequency. If node x was assigned to node y in more than 5 control subjects (across all time point

intervals, i.e., $> 5\%$ of the time), we remove this entry from the permutation matrices of all stroke subjects. All remaining entries after this removal procedure are considered as significant remappings. The rationale for this thresholding approach is that there may be remapping that happens longitudinally in controls that is either due to noise in the fMRI data or some other physiological noise that is unrelated to stroke recovery. Removal of these normative effects will allow better isolation of remapping likely to be related to the post-stroke reorganization process. Because using the cutoff of 5 control subjects is an arbitrary choice, we have replicated the main analyses using a cutoff of 1 (i.e., remove remap of node x to node y from stroke subjects if node x was assigned to node y in 1 or more control subjects (across all time point intervals, i.e., $> 1\%$ of the time). The results with this more conservative threshold are provided in the supplementary materials, and are very similar to the main results (Figure S16, S17, S18).

The permutation matrices, calculated for each pair of time points, were then used to quantify functional reorganization. We defined functional remapping at three levels:

- **Subject level:** To assess the amount of functional reorganization in an individual, the number nodes that were remapped (sum of the off-diagonal in P) between each time point interval was calculated. This referred to as the 'number of remaps' between subsequent imaging sessions for a single subject.
- **Node level:** To assess the spatial pattern of reorganization across the brain, we calculated each node's 'remap frequency', i.e. the proportion of individuals that had that brain region remap between two subsequent time points.

- **Network level:** To assess the network-level pattern of reorganization, we calculated the sum of remaps within and between 8 functional brain networks across all subjects. Since there are 8 networks, there are 64 possible source network/target network combinations (including the phenomenon of a node in a network remapping to a different node within the same network). We normalized each sum by the number of subjects, and then by the number of nodes in the source network. This value therefore expresses the proportion of remaps between networks, per subject, adjusted for the total number of possible remaps in each network.

1.2.9 Statistical analyses

To test the hypothesis that brain regions more structurally disconnected by the stroke lesion would have more frequent remapping, we calculated the correlation between the node remapping frequency and the sample median log-transformed ChaCo scores that quantify the regional amount of white matter connectivity disruption due to the stroke lesion. We removed nodes which had non-zero overlap with each subject's lesion in the calculation of the median ChaCo score to exclude the effect of direct damage from the lesion. To test the hypothesis that brain regions more functionally disconnected by the stroke lesion would have more frequent remapping, we calculated the correlation between the node remapping frequency and the t-statistic of the node strength. The statistical significance of the correlations described above were assessed with permutation testing.

There are four subject-level remapping values for each subject, representing 4 time point comparisons post-stroke: 1 week - 2 weeks, 2 weeks - 1 month, 1 month - 3 months and 3 months - 6 months. Because there was a statistically significant correlation between scan length and remapping for the time point from 1 week - 2 weeks post-stroke (Figure S4), the fMRI scan lengths of both time points were included as covariates in analyses concerning remapping over time.

To test the hypothesis that individuals with more baseline remapping would have greater initial motor impairment, we calculated the Pearson correlation between Fugl-Meyer motor scores at 1 week post-stroke and subject-level remapping from 1 week to 2 weeks post-stroke. To test the hypothesis that individuals with more baseline remapping would have greater motor recovery at 6 months, we calculated the Pearson correlation between the change in Fugl-Meyer motor scores from 1 week to 6 months post-stroke and subject-level remapping from 1 week to 2 weeks post-stroke.

To test the hypothesis that individuals with more remapping from one time point to another have better motor improvement, we calculated the Pearson correlation between change in Fugl-Meyer motor scores and subject-level remapping from one time point to the next for all four pairs of subsequent time points. This analysis enables us to identify whether remapping within a particular time point interval is more or less associated with motor improvement. In order to leverage the repeated subject measurements, a linear mixed effects regression model was employed to determine the relationship between the amount of remapping between sessions and the change Fugl-Meyer score between sessions, including age, sex, and scan length as covariates. Let i index a subject, t_{ab} index a time

point interval (t_a = first time point, t_b = second time point, and t_{ab} = the time point interval). Our model is then (split across 2 lines):

$$\begin{aligned} changeFM_{it_{ab}} = & \beta_0 + \beta_1 remapping_{it_{ab}} + \\ & \beta_2 scanlength_{it_a} + \beta_3 scanlength_{it_b} + \beta_4 age_i + \beta_5 sex_i + b_i + \epsilon_{it_{ab}} \end{aligned}$$

where $b_i \sim N(0, \sigma_1^2)$ and $\epsilon_{it_{ab}} \sim N(0, \sigma_2^2)$. We include the random effect b_i to account for correlation within a subject at different time points.

1.2.10 Code availability

The code for to replicate this analysis is available on GitHub:
<https://github.com/emilyolafson/stroke-graph-matching>

1.3 Results

1.3.1 Functional reorganization is primarily observed in the brainstem and cerebellum

At the node level, remapping occurred most often in the brainstem and cerebellum (Figure 1.3A,B), similar to the spatial distribution of median ChaCo scores (amount of structural disconnection) across the stroke sample, which were also highest in the brainstem and cerebellum (Figure 1.2C). We also calculated

group-level structural connectivity disruption in an approach more analogous to node remapping, by binarizing ChaCo scores into 'disrupted' and 'nondisrupted' nodes and calculating frequency of disrupted nodes over the population, with similar results (Figure S5). For this paper, regional ChaCo scores were chosen over disconnection frequencies in order to preserve information about the magnitude of the disconnection. We hypothesize that the magnitude of disconnection influences whether a region is remapped or not.

Next, we assessed network-level remapping within 8 functional networks. The most remaps were observed in the subcortical-cerebellum network (Figure 1.3C,D) and in particular between contralateral nodes in the subcortical/cerebellum network (Figure S6).

Figure 1.3: Visualization of node-level remapping frequencies and group-level structural connectivity disruptions due to the lesion.

A. Node remap frequencies are plotted on a glass brain averaged across 4 time point comparisons (only displaying values above 0.1, for clarity). Inset figures display a lateral view (top row) and medial view (bottom row). **B.** Node remap frequencies > 0.1 plotted on a glass brain, displayed separately for each time point comparison. **C.** Network-level sum of remaps. Remaps are separated based on their position relative to the lesion (contralesional vs. ipsilesional). **D.** Network-level sum of remaps, displayed separately for each time point comparison. Ipsilesional = same hemisphere as the lesion, contralesional = opposite hemisphere as the lesion

A

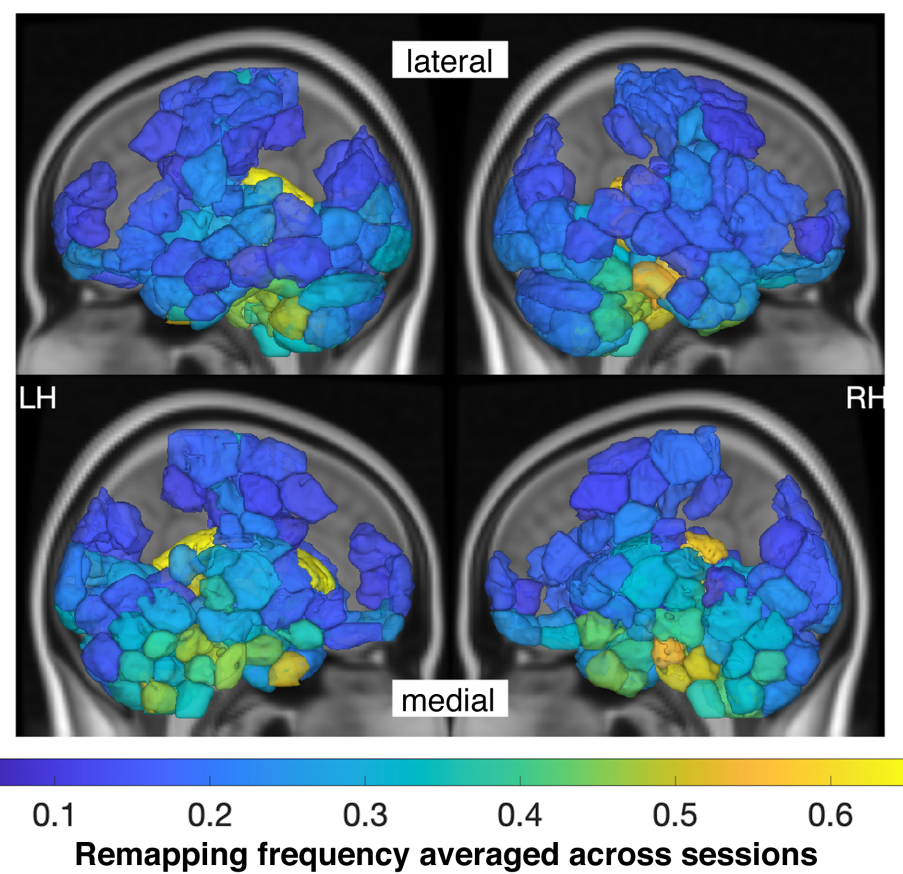


Figure 1.3 (Continued)

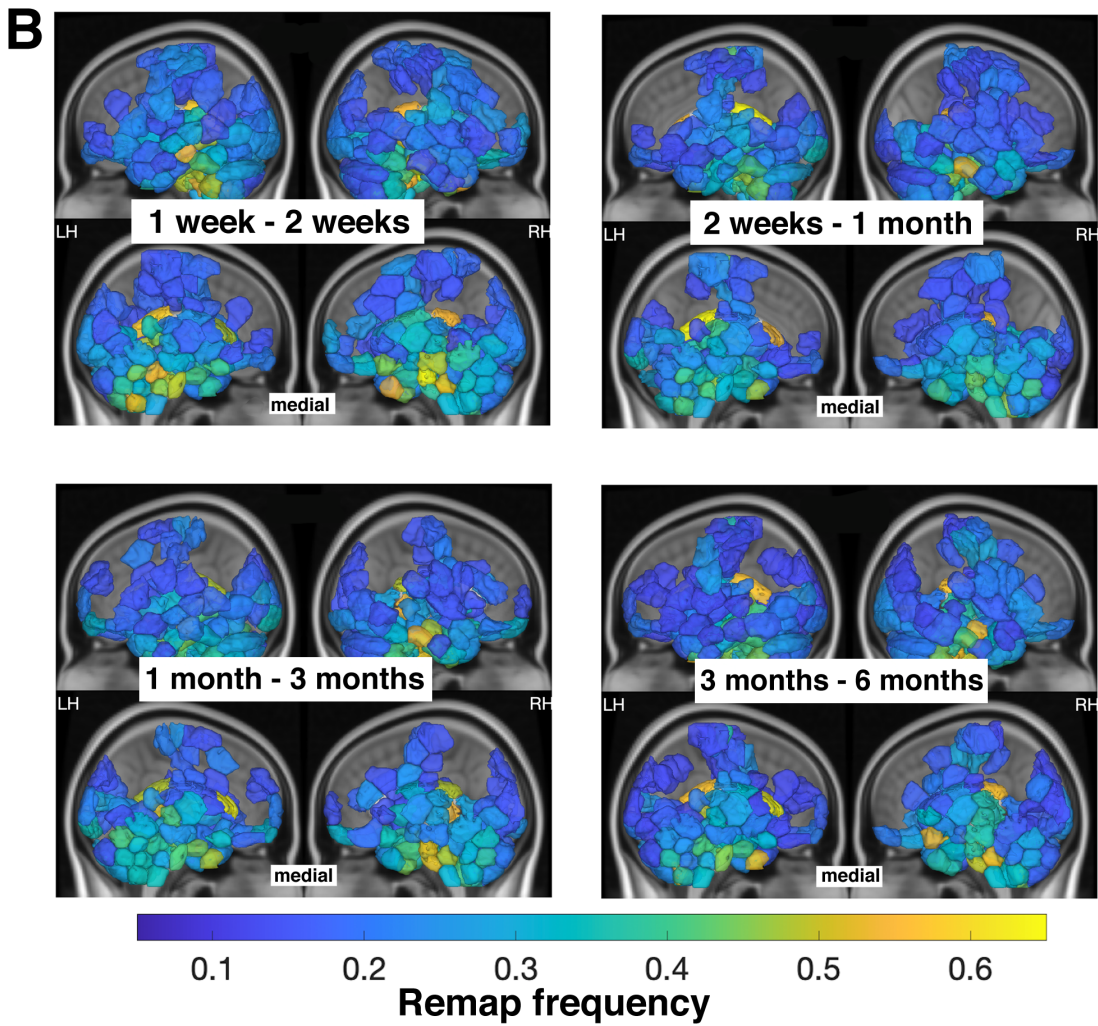


Figure 1.3 (Continued)

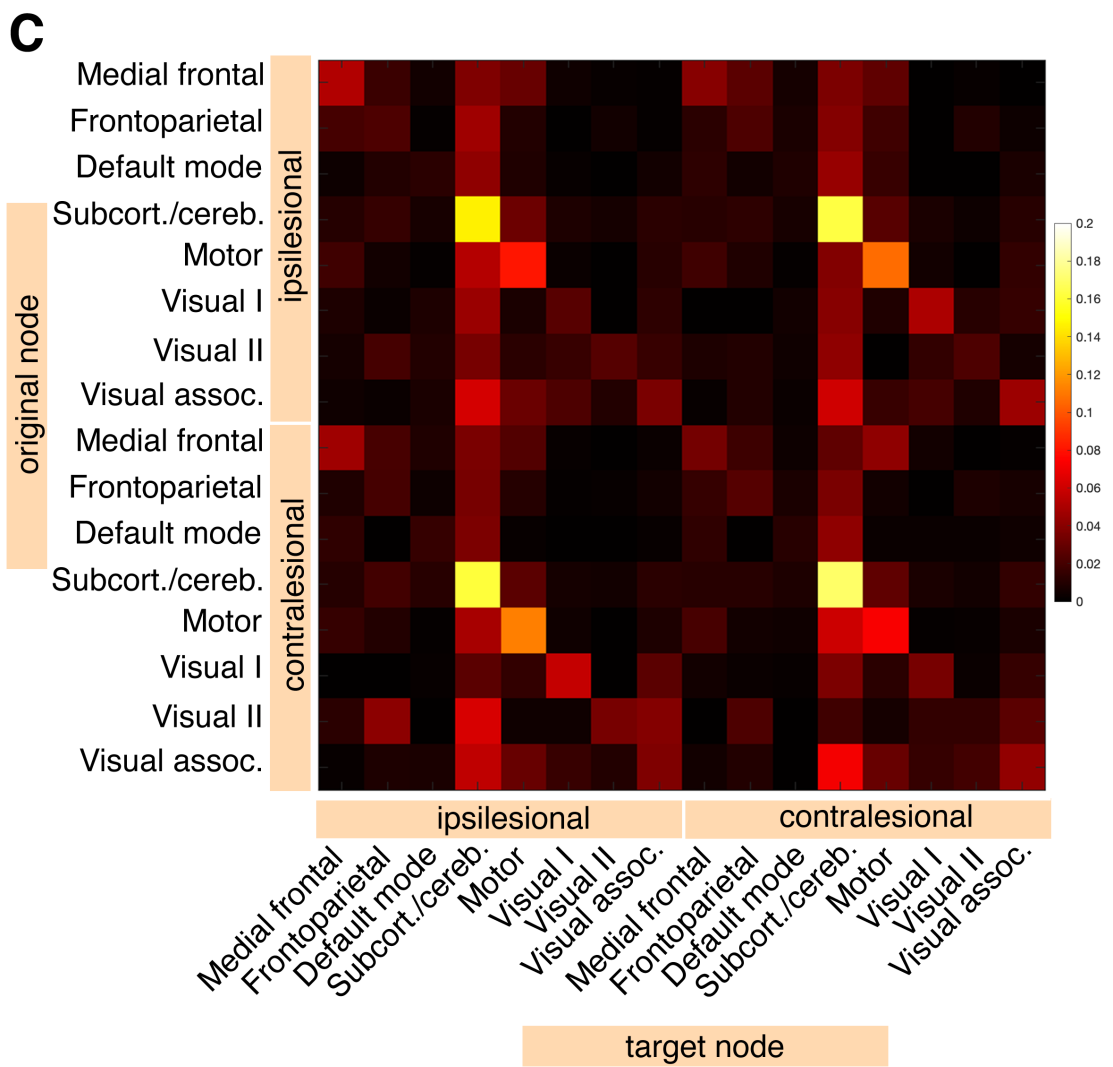


Figure 1.3 (Continued)

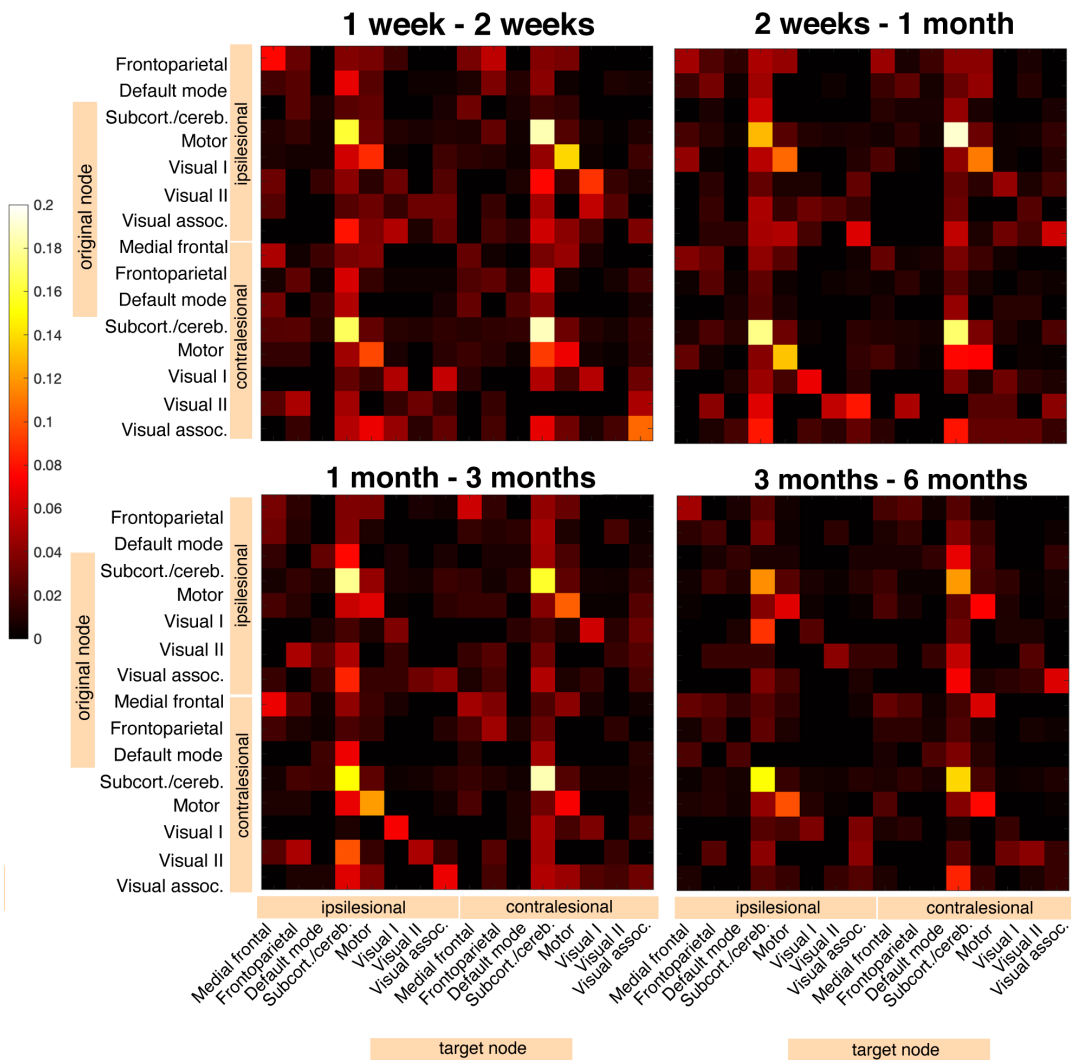
D

Figure 1.3 (Continued)

1.3.2 Regions with greater structural and functional disconnection have more functional reorganization over time

There was a significant, positive correlation between node remapping frequency and median regional ChaCo scores from 1 to 2 weeks post-stroke ($r = 0.22$, $p = 3.05\text{e-}4$), such that those regions with more structural connectivity disruption across the stroke subjects also had more remapping over time (Figure 1.4A). This relationship was observed across all time points (Figure S7A), and furthermore, across subjects, the brain regions that remap have significantly higher ChaCo scores compared to those that do not remap (assessed with permutation testing with 10000 permutations) (Figure S7B).

On the other hand, node remapping frequency at 1-2 weeks post stroke was negatively correlated with node strength relative to healthy controls at 1 week post-stroke ($r = -0.44$, $p = 2.62\text{e-}14$) (Figure 1.4B), where regions with lower node strength relative to controls at 1 week underwent the most remapping between 1-2 weeks post-stroke. This relationship was present across all time points (Figure S10, S11, S12) and the correlation is very similar when using the first or second node strength measurement (Figure S9).

The nodes that underwent the most remapping were the most structurally and functionally disconnected, but the relationship between structural and functional disconnection is non-linear (Figure 1.4C). Instead, the relationship between SC and FC disruption is impacted by the magnitude of the structural disruption. As seen in Figure S8, there is a clear cutoff for regions consistently structurally disrupted across subjects, corresponding to a ChaCo score of 0.003 ($\log(\text{ChaCo})$ of -6). For regions exceeding a ChaCo score of 0.003 (i.e., with high structural

connectivity disruption), there was a significant negative correlation between relative node strength and ChaCo scores ($r = -0.50$, $p = 2.1\text{e-}6$)(Figure 1.4D) and for regions below a ChaCo score of 0.003 (i.e., with little/no structural connectivity disruption), there was a significant positive correlation between relative node strength and ChaCo scores ($r = 0.49$, $p = 4.78\text{e-}13$)(Figure 1.4E).

Figure 1.4: Relationships between FC disruption, SC disruption, and remapping over the 1 week - 2 week time interval post-stroke.

A. Correlation between node remapping frequency and t-statistic of node strength. A jitter of 0.01 was added to data points along the x-axis to increase visibility. **B.** Correlation between node remapping frequency and ChaCo scores. A jitter of 0.01 was added to data points along the x-axis to increase visibility. **C.** Correlation between t-statistic of node strength and ChaCo scores. Dashed horizontal line at $y = -6$ represents the cut off point of $\log(\text{ChaCo}) - 6$, representing more SC disruption shown in **D**, below -6 representing minimal SC disruption is shown in **E**.

● Medial frontal ● Frontoparietal ● Default mode ● Subcortical-cerebellum
● Motor ● Visual I ● Visual II ● Visual association

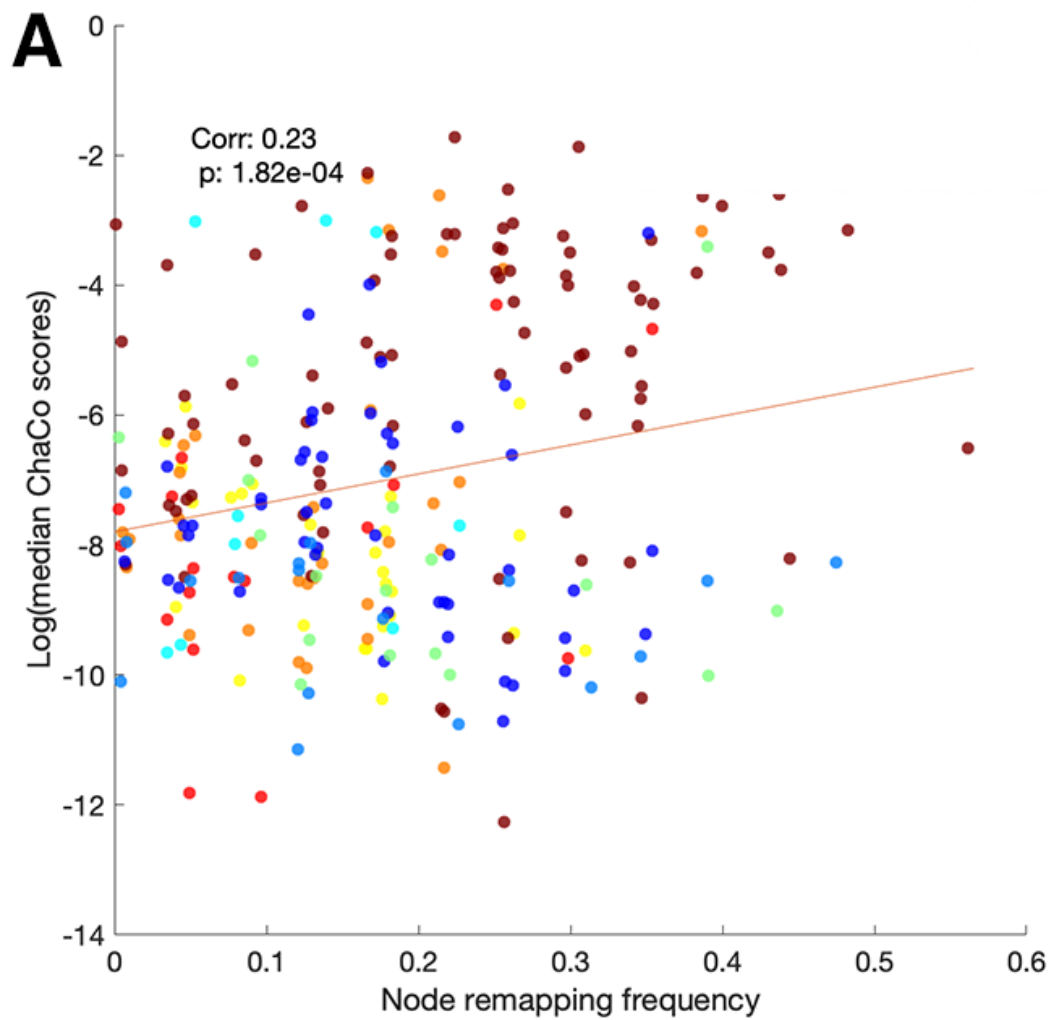


Figure 1.4 (Continued)

• Medial frontal • Frontoparietal • Default mode • Subcortical-cerebellum
 • Motor • Visual I • Visual II • Visual association

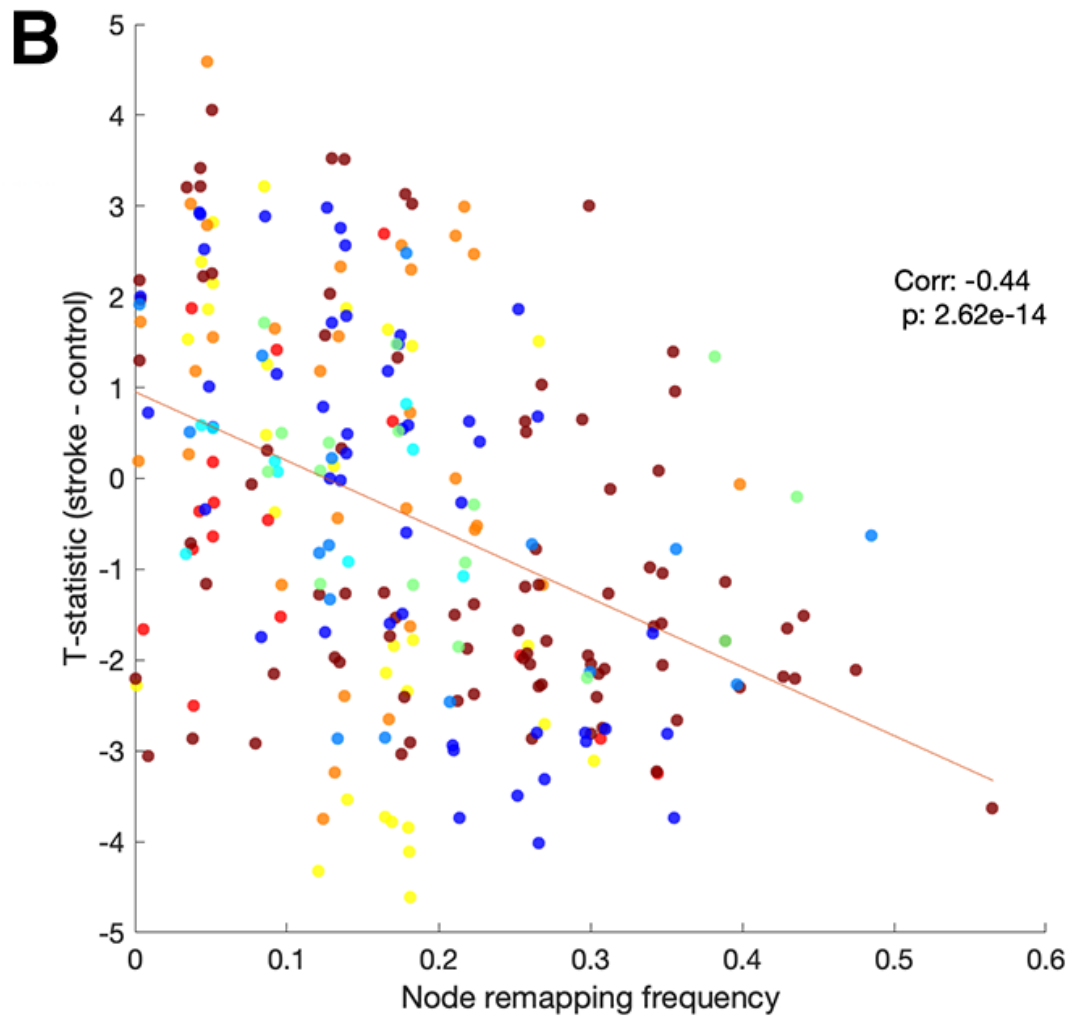


Figure 1.4 (Continued)

● Medial frontal ● Frontoparietal ● Default mode ● Subcortical-cerebellum
 ● Motor ● Visual I ● Visual II ● Visual association

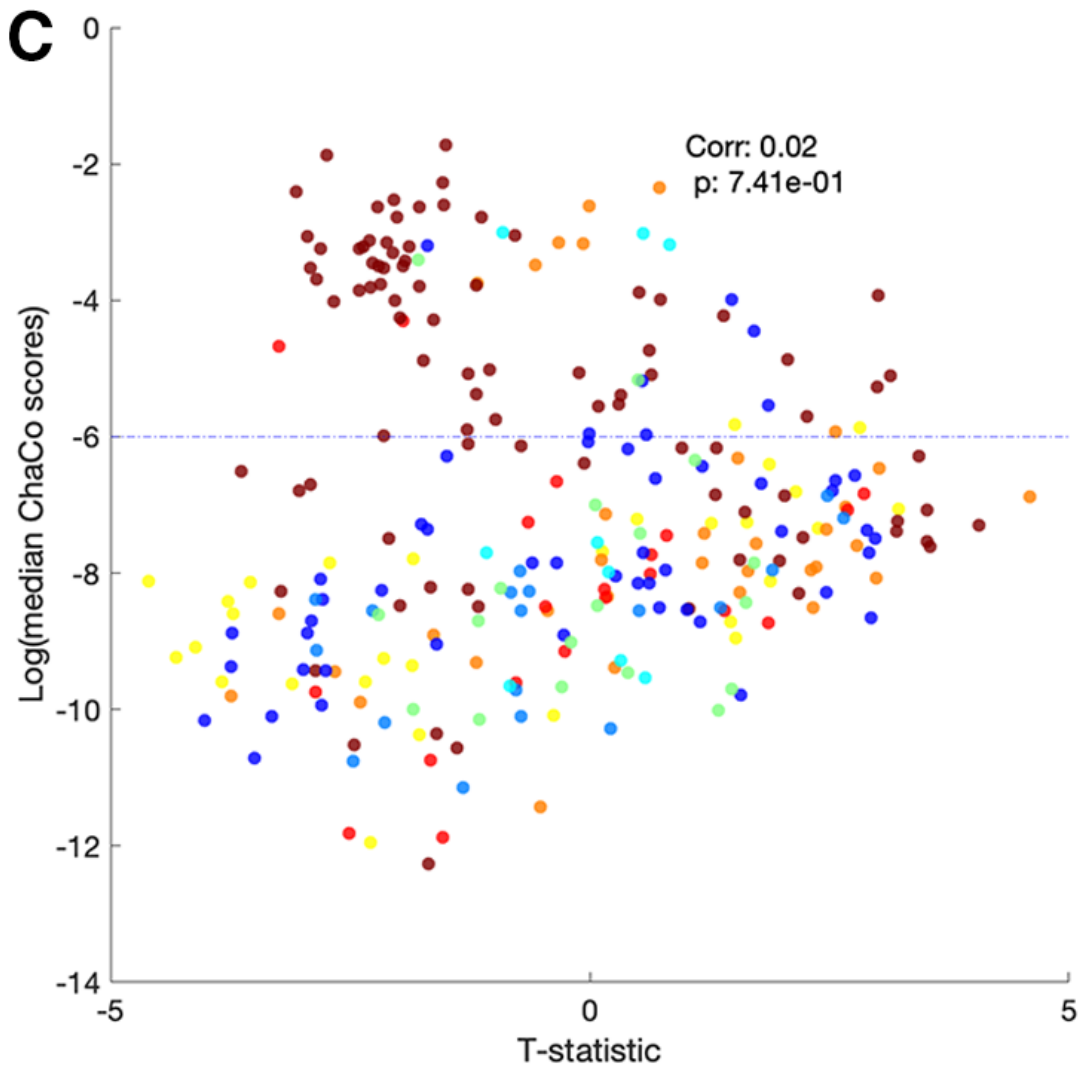


Figure 1.4 (Continued)

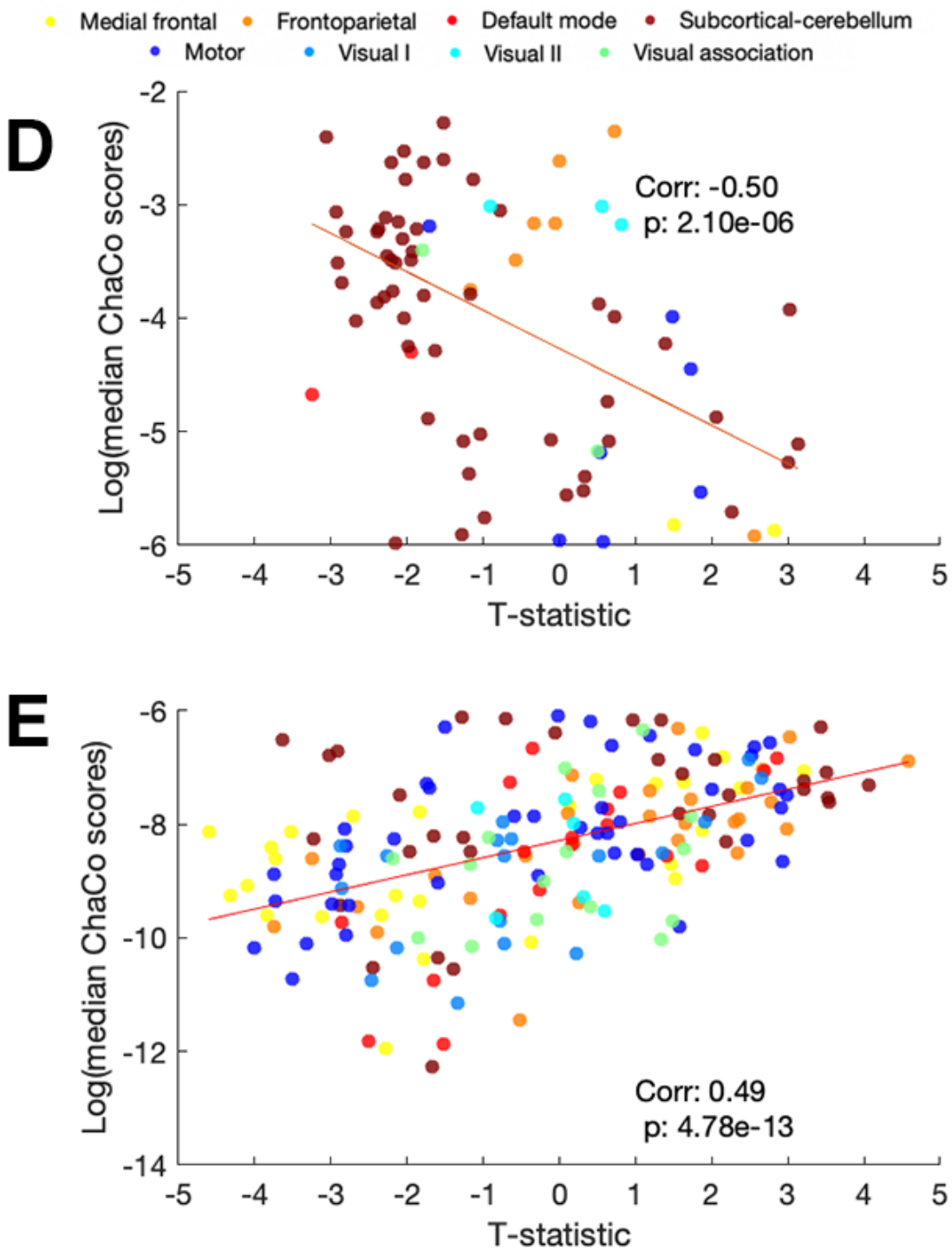


Figure 1.4 (Continued)

1.3.3 Functional reorganization is related to impairment and recovery

We observed a significant positive correlation between subject-level early post-stroke remaps (between 1 weeks and 2 weeks post-stroke) and the 6 month improvement in motor scores, as measured by the difference in Fugl-Meyer scores at 6 months and 1 week post stroke (controlling for scan lengths). This result indicates that individuals with more early functional remapping had better long-term recovery (Figure 1.5A). There was also a significant negative relationship between the number of early post-stroke remaps (between 1 week and 2 weeks) and baseline Fugl-Meyer scores, such that more impaired subjects had more remapping at baseline (Figure 1.5B). The linear mixed effects model demonstrated a statistically significant relationship between 'remapping' and change in Fugl-Meyer score. For every one unit increase in 'remapping', there is an average increase of 0.15 units in the change in Fugl-Meyer scores, holding all other factors constant ($p = 0.006$) (Figure 1.5C). The amount of recovery between subsequent sessions was positively associated with the number of remaps between sessions for the two comparisons between 1 week and 2 weeks post-stroke (Figure 1.5D), but only a trend for significance existed at the 2 weeks to 1 month time points and there was no significant correlation for the 3 and 6 months comparison.

Figure 1.5: Relationship between subject-level remapping, baseline motor impairment, eventual motor recovery.

Subject-level remapping is related to baseline motor impairment and eventual motor recovery. **A.** Pearson correlation between subject-level remaps between 1 week and 2 weeks post stroke and change in Fugl-Meyer scores between 1 week and 6 months post-stroke. **B.** Pearson correlation between subject-level remaps between 1 week FC and 2 week FC and 1 week Fugl-Meyer scores, controlling for scan lengths at 1 week post-stroke at 2 weeks post stroke. **C.** Results from linear mixed effects analysis; each color indicates a different individuals' longitudinal time point. **D.** Pearson correlation subject-level remaps for each pair of time points and the change in Fugl-Meyer scores between time points, controlling for the scan length of the 2 scans in the remapping calculation.

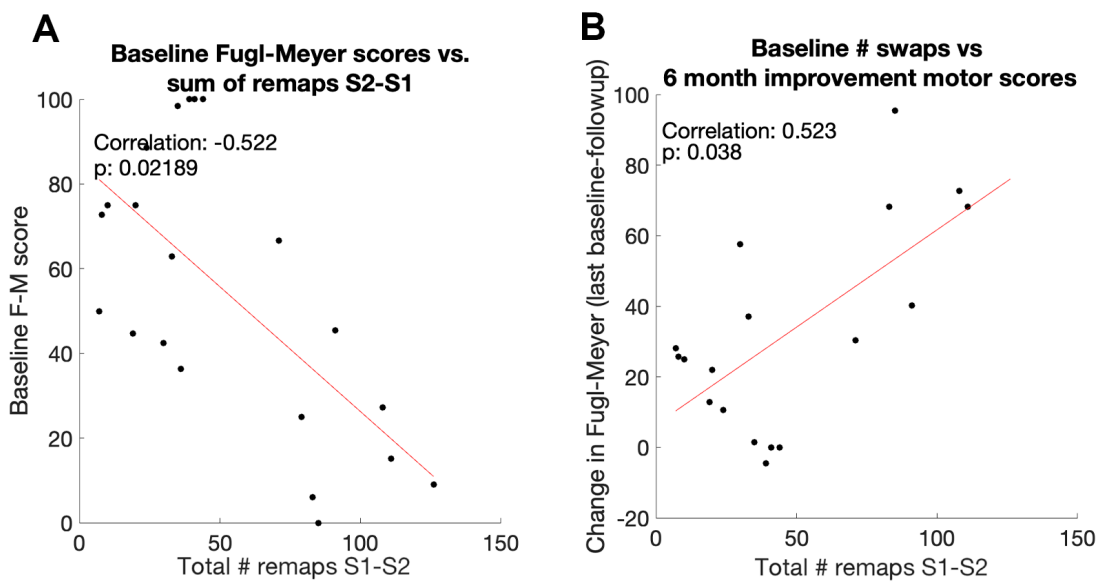
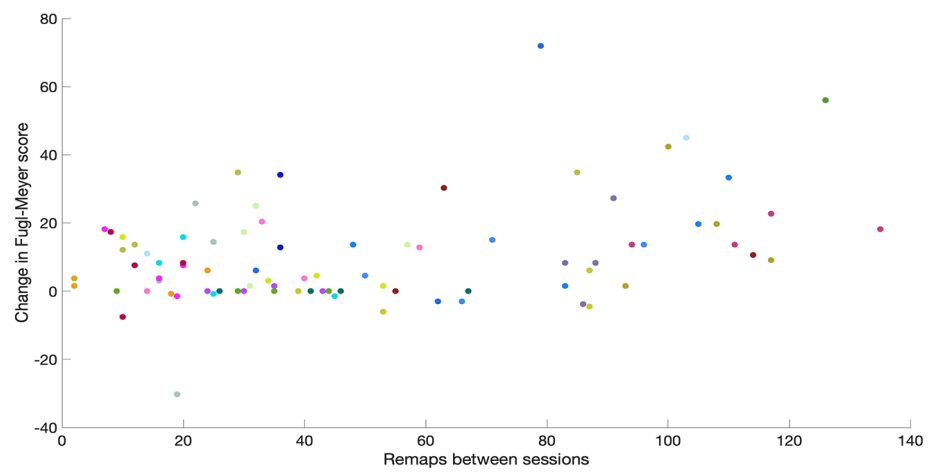


Figure 1.5 (Continued)

C

	Estimate	Std. Error	t-statistic	p
Intercept	21.498	14.983	1.435	0.155
Remapping	0.153	0.055	2.8	0.006
Age	-0.229	0.175	-1.31	0.194
Sex	-2.514	3.61	-0.696	0.488
Lesion volume	0	0.002	-0.158	0.875
Scan length - 1st scan	-0.05	0.033	-1.506	0.136
Scan length - 2nd scan	0.033	0.031	1.075	0.286

Figure 1.5 (Continued)

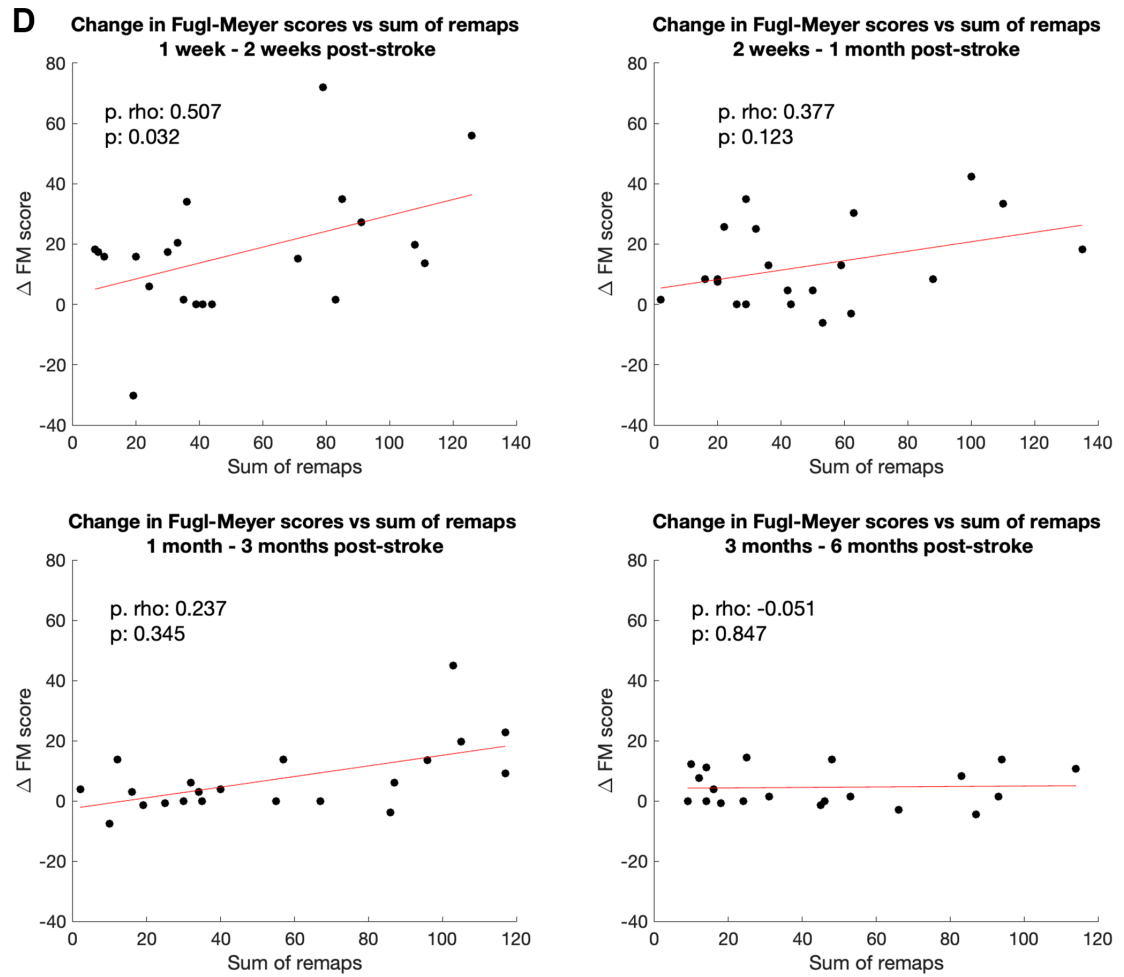


Figure 1.5 (Continued)

1.3.4 Robustness of results

The maximum overlap of lesions with each ROI is no more than 30 percent (Figure S19) and, importantly, lesioned voxels were excluded from FC calculations. We also found that the number of remaps was not related to differences in in-scanner motion between scans, as measured by framewise displacement (Fig S20).

1.4 Discussion

In this paper we proposed a measure of functional connectome reorganization based on graph matching and evaluated its relationship to structural & functional disconnection and motor impairment/recovery in a set of 23 individuals with pontine stroke. We observed instances of functional reorganization over the 1 week to 6 months post-stroke period and demonstrated that the areas that undergo functional reorganization most frequently are in cerebellar/subcortical and motor networks. Furthermore, regions more impacted by stroke via disruption to their structural and functional connections had more functional remapping over time. Finally, we show that functional reorganization one week post-stroke is highly related to both baseline impairment and the extent of motor recovery at 6 months, and, finally, that the extent of functional reorganization between 1 week and 2 weeks post-stroke is correlated with the extent of motor recovery observed in this same subacute time period.

We first note that remaps, defined in this paper as instances where a node is assigned to a different node longitudinally in the linear assignment algorithm,

were observed in the control population. This ‘noise’ may be related to inherent variability in subject-level functional connectivity, acquisition-related noise, or a combination of both. Graph matching has recently been used to develop a measure of connectome similarity within healthy controls (Osmanlioglu et al. 2020). Consistent with our findings, Osmanlioglu and colleagues observe that graph matching using the same subject’s functional connectomes acquired during different scans is imperfect, i.e., on average there are several remaps in a single subject’s functional connectomes, suggesting that functional network structure in the same individual over time is variable. To discern the difference between natural individual variability in functional connectivity and signal, we removed all remaps that were observed in more than 5 control subjects. Almost certainly, we have not completely isolated the influence of natural individual variability; this methodology can likely be improved with future studies investigating graph matching patterns within larger populations of healthy individuals. Scan duration also influences functional connectome similarity in healthy controls, driven by the lower SNR of shorter scans. Accordingly, we observed a relationship between subject-level remaps and scan length, such that subjects with shorter scans had more remaps. To account for this influence, we included scan duration - first and second scan length - as covariates in all longitudinal analyses, but future studies should attempt to obtain consistent scan durations for all subjects.

Motor recovery following stroke is supported by active functional and structural remodelling in the area bordering the stroke, including increases in excitability, increases in dendritic spine turnover, and the formation of new axonal projections (Murphy and Corbett 2009). This remodelling can entail surviving cortical areas remapping functionally to compensate for post-stroke impairment (Brown et al. 2009). The dynamic reorganization of resting-state functional con-

nectivity, observed in this stroke cohort in subcortical and cerebellar areas, may reflect longitudinal compensatory changes in representations of motor functions. Interestingly, we showed correlations between amount of functional remapping and amount of motor improvement but only in the period of time in which most post-stroke recovery occurs (within 3 months after stroke) (Lee et al. 2015). However, resting-state functional connectivity may not be fully representative of brain activation patterns underlying specific behaviors (i.e. during a task), and has shown to be constrained by the structural connectome (Kuceyeski et al. 2019; Honey et al. 2009). Thus, it is possible that the remapping observed is not a functional remapping per se (in the sense of remapping a region's role in a specific task), but a shift in balance of a brain area's functional connectivity profile at rest, which could reflect task-based functional compensations, changes in network topology, and/or underlying structural remodelling.

We now understand that deficits arising from stroke are not only related to the damage inflicted at the stroke core, but also to remote cortical areas structurally connected to the lesion, due to retro- and anterograde degeneration (Guggisberg et al. 2019). For instance, several studies have shown that there are local reductions in cortical thickness in areas directly connected to subcortical lesions (Duering et al. 2015; Cheng et al. 2015). These degenerative changes are long-term effects of a stroke. We showed that structural disconnection from a stroke lesion is associated with remapping even at 6 months post-stroke, suggesting that late-stage impacts of the stroke may trigger functional reorganization.

However, as stated earlier, recovery-related reorganization usually occurs within the first three months post-stroke. We observed recovery-related remapping primarily in the acute period (1-2 weeks after stroke), where there was also a

significant correlation between structural connectome disruption and remapping as well as functional connectome disruption and remapping. Structural connectivity disruption between nodes has been linked to perturbations of functional connectivity (FC) within the first 2-4 weeks after stroke (Griffis et al. 2019, 2020; Wodeyar et al. 2020), including by Lu and colleagues (2011), who demonstrated that pontine strokes disrupt FC between the cortex and the cerebellum. These papers generally show that damage to structural connections between nodes, direct or indirect, is associated with reductions in FC between those nodes. We observed that remapping more frequently occurs in nodes with greater structural and functional connectivity disruption due to the stroke. We observed that functional connectivity changes were related to structural connectivity disruption magnitude; nodes with more structural connectivity disruption had a negative relationship with changes in node strength, where more SC disruption was related to weaker FC. These nodes, overwhelmingly a part of the subcortical/cerebellum network, also have the highest levels of remapping. On the other hand, regions with lower structural connectivity disruption have a positive relationship with changes in node strength, where less SC disruption is associated with higher node strength. This result suggests that remapping after pontine stroke may be a mechanism that occurs to only the most severely disrupted brain regions, whose structural connections have been damaged to the point of weakened FC, whereas regions with less structural disruption can compensate for the damage in the form of upregulated FC.

Pontine strokes primarily affect large-diameter projection fibers, which tend to produce more severe functional connectivity deficits when damaged (Griffis et al. 2020). Brain regions that were once structurally and functionally connected via these fibers may remap more often as their role in the network is taken over

by other nodes with more preserved structural connections. For instance, Lu et al. 2011 demonstrated reduced FC between the motor cortex and cerebellum in subjects whose cortico-ponto-cerebellar fibers were damaged from pontine stroke. Regions in the cerebellum and motor cortex that can no longer communicate via these fibers may remap to other nodes with preserved cortical/cerebellum connectivity.

Other factors may make regions more or less amenable to remapping; perhaps a region is better positioned within the network to assume lost functionality, such as in the cerebellum where there is considerable redundancy in the somatotopic layout (Mottolese et al. 2013) which may enable it to compensate more easily for lost functionality.

We also show that more remapping between sessions is associated with better motor recovery between those same sessions, and that more remapping in the early phase of stroke is related to both amount of baseline impairment and the degree of motor recovery at 6 months. Functional reorganization measured with this remapping technique may be interpreted as reflecting a compensatory, beneficial process that is proportional to the extent of motor recovery. On the other hand, this approach may also be capturing phenomena that occurs during the first 6 months after stroke that are unrelated to recovered functionality, but that correlate with measures of recovery nonetheless. For instance, stroke-related increases in noise in the subcortical/cerebellum network may result in more remapping which could be the result of a random or pathological process concomitant with a recovery mechanism. Thus, more densely-sampled fMRI studies should be performed to identify other elements of this reorganization process.

The most remaps were observed in the subcortical/cerebellum network, suggesting that remapping is likely reflecting a process of functional reorganization that is spatially constrained (Figure ??). This network-level reorganization is consistent with prior task-based studies showing remapping of motor-based activations to premotor and homologous areas, and with studies of resting-state FC that demonstrate specific spatial patterns of FC changes after stroke, like changes in resting state FC within motor networks (Zhang et al. 2016), and contralateral functional connectivity changes that are concentrated in a small set of brain regions (Yourganov et al. 2021).

1.4.1 Limitations

There are several limitations to this study. The first is sample size, which is partially mediated by the frequency of the longitudinal sampling and the homogeneity of the population. The second is that the impact of fMRI noise in the remapping procedure cannot be completely accounted for. We do see that some nodes with high frequency remapping are also those that have lower SNR in the fMRI data; generally, the SNR of fMRI is lowest in medial structures such as the thalamus, cortical midsurface, and most consequentially to this study, the cerebellum. Thus, it is possible that noise contamination was captured in the graph matching procedure and has leaked into the results. Our approach of using the arguably more noisy control data to filter this potential source of noise helped mitigate this drawback. Second, structural disconnection metrics were obtained for each individual using indirect methods (i.e. the Network Modification Tool), instead of directly from diffusion MRI in the individuals with stroke. Third, the correlation between baseline and long-term recovery in stroke subjects is

generally high (Krakauer and Marshall 2015); because of the small sample size in this study, it is not possible to discern whether the relationship between early remapping and 6 month recovery holds while controlling for initial impairment. Fourth, we did not have data available regarding the rehabilitation program, as it was not collected at the time of fMRI scanning and motor assessments, so the effect of rehabilitation could not be accounted for.

1.5 Conclusion

In this study we proposed a measure of functional connectome reorganization, called remapping, and applied it to longitudinal resting-state fMRI data in a cohort of pontine stroke patients. Remapping was observed in all stroke subjects and was correlated with recovery over the early to late subacute phases. Areas impacted by the lesion through structural disconnection were more likely to remap than those areas not impacted by the lesion. This work expands our understanding of functional processes related to recovery after stroke, and future studies should examine remapping in other populations beyond pontine stroke subjects, such as those with cortical stroke. If we can identify subjects who have more potential for functional reorganization, or can devise therapeutics to boost this remapping mechanism, we may be able to improve patient outcomes after stroke.

CHAPTER 2

FRONTOPARIETAL NETWORK ACTIVATION IS ASSOCIATED WITH MOTOR RECOVERY IN ISCHEMIC STROKE PATIENTS*

2.1 Introduction

The ability to perform motor functions after stroke depends on the coordinated reconfiguration of distinct global brain activity patterns (Park et al. 2011). Novel data-driven techniques to characterize whole-brain activity in functional magnetic resonance imaging (fMRI) scans at single-frame resolutions have illuminated the dynamic nature of brain activity in several brain disorders (**Parker-Singleton-ur**; Braun et al. 2021; Adhikari et al. 2020; Kaiser et al. 2019), but methods assigning each time point to a discrete state have not yet been applied to examine altered brain dynamics in stroke patients. These methods provide information about brain function complementary to and beyond traditional static measures of functional connectivity (Cornblath et al. 2020), and thus may provide new insights regarding the process of recovery following stroke.

Prior work characterizing spatiotemporal brain dynamics after stroke has focused on identifying altered functional connectivity states, which reflect time-varying patterns of functional connectivity (FC). Dynamic FC analyses identify recurrent connectivity patterns using a sliding window approach, in which FC is

* Olafson, E., Russello, G., Jamison, K. W., Liu, H., Wang, D., Bruss, J. E., Boes, A. D., Kuceyeski, A. (2022). Frontoparietal network activation is associated with motor recovery in ischemic stroke patients. *Communications Biology*, 5(1), 993.

repeatedly calculated over consecutive windowed segments of the fMRI scan. This approach yields FC networks that fluctuate over time, with a temporal resolution proportional to the size of the window; about 30-60 seconds (Savva, Mitsis, and Matsopoulos 2019). In stroke populations, dynamic FC studies have demonstrated stroke-related differences in temporal configurations of motor networks (Bonkhoff et al. 2020a) and participation in connectivity states that varies with severity (Bonkhoff et al. 2020b).

In contrast, analysis at a single relaxation time (TR) resolution of activation states identified in a data-driven fashion using k-means clustering of the time series data (Cornblath et al. 2020) provides a closer look at the moment-to-moment changes in recurrent brain activity, with the time spent in each state lasting, on average, 5-10 seconds (Cornblath et al. 2020). A benefit to analysing brain activation states over or alongside connectivity states is that activation patterns can enable a more refined interpretation of connectivity differences between groups. FC is traditionally defined as the correlation between two brain region's activity over time. FC may be driven by two distinct features of brain activity: by the individualized spatial patterns of large-amplitude activations (Zamani Esfahlani et al. 2020), and by the amount of time spent in recurring patterns of activity (Betzel et al. 2021; Baker et al. 2014). In this paper we aim to identify group-level patterns of brain activity after stroke that relate to recovery, and assume that recurring activity patterns are shared across individuals but are expressed in different proportions. Understanding the temporal patterns of activity underlying recovery-relevant FC changes after stroke can aid in the development of more accurate targets in stimulation therapies.

Recent work has highlighted the importance of frontoparietal areas in supporting motor abilities in the chronic phase of stroke (Tscherpel et al. 2020; Hensel et al. 2022) specifically in patients with poor corticospinal tract (CST) integrity (Hordacre et al. 2021). When these descending motor pathways are significantly damaged, descending white matter tracts from higher-order motor areas, like regions of the frontoparietal network (FPN), may support motor output. Because of the differential use of the dominant and non-dominant arm throughout life, we were interested in determining whether handedness relative to the lesioned hemisphere would modify the recruitment of a frontoparietal state to promote motor recovery. Understanding this type of subject- and lesion-specific variability in the post-stroke recovery process is precisely the type of information needed to develop personalized rehabilitation strategies to maximally promote recovery.

Here, we propose to first identify and characterize recurring brain activity patterns, or states, in healthy controls and individuals with ischemic pontine stroke (Cornblath et al. 2020). We hypothesized that individuals with ischemic stroke would display altered dynamic brain state metrics, e.g. fractional occupancy, dwell time and appearance rates, compared to control subjects, and, further, that these dynamic state metrics would be associated with measures of motor recovery. In an exploratory analysis, we examined whether time spent in a brain state characterized by frontoparietal activation would be differentially recruited for later-stage motor recovery depending on the side of the lesion relative to the subject's handedness. Finally, to bridge dynamic brain state analyses and more classic functional connectivity approaches, we assessed the relationship between the amount of time spent in different brain states and the FC between several resting-state networks. This last analysis is particularly important in terms of linking our current findings to previous studies of how rehabilitation techniques,

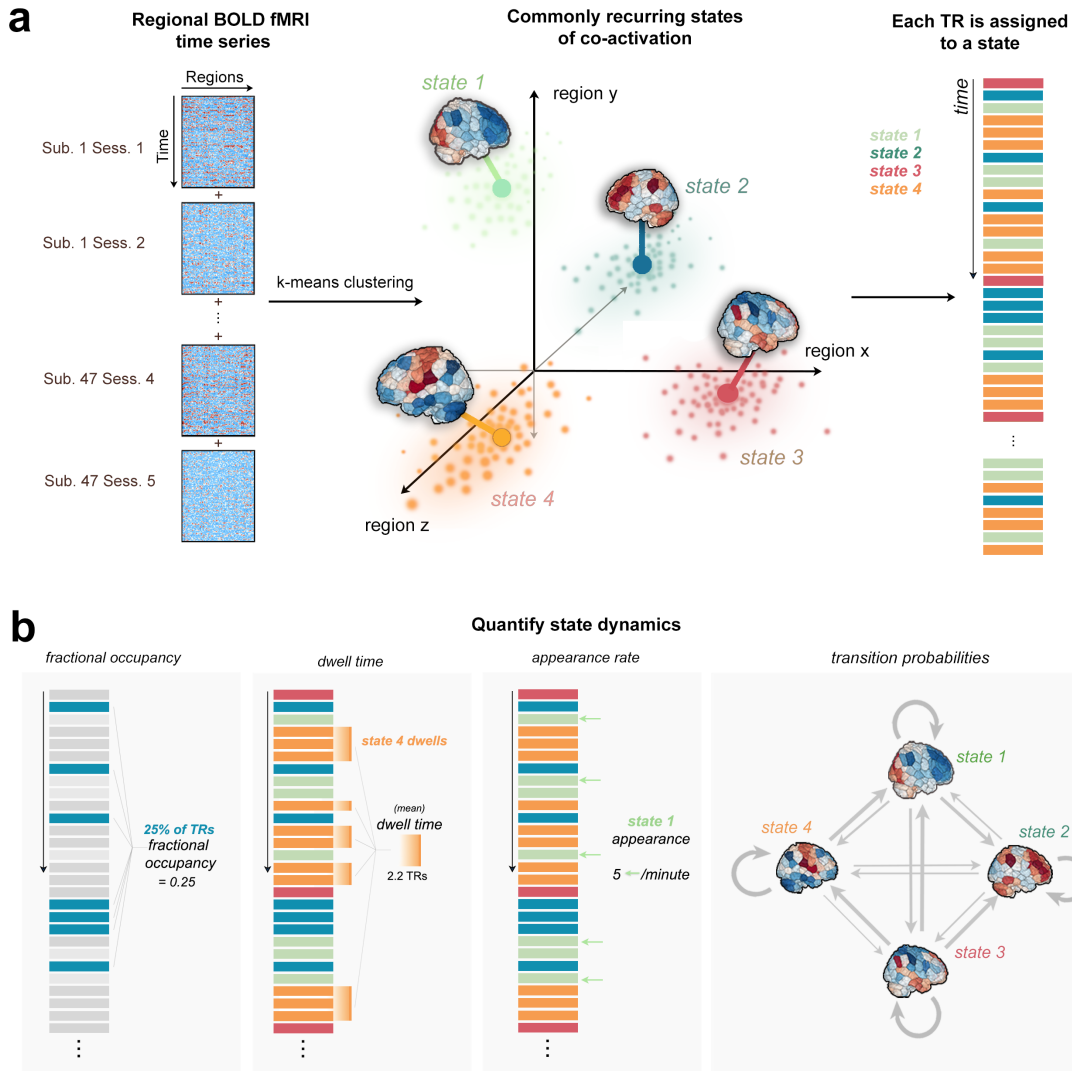


Figure 2.1: Clustering of time series data and quantification of dynamic state metrics. **a.** Time series data from all subjects were concatenated together along the time dimension. K-means clustering produced 4 distinct brain activation states defined by different locations in regional activation space (image adapted from Cornblath et al. 2020). Each TR is assigned to one of four brain states based on k-means partitions. **b.** Fractional occupancy, dwell time, appearance rate, and transition probabilities are calculated separately for each subject and for each state.

including non-invasive brain stimulation, modulate the functional connectome and possibly motor recovery.

2.2 Methods

Data description

The data consist of 23 first-episode stroke patients (34-74 years old; mean age 57 years; 8 female) with isolated pontine infarcts and 24 healthy sex-matched controls (33-65 years old; mean age 52 years; 10 female). A subset of the data (11 stroke subjects and 11 healthy control subjects) used here has been previously described in Lu et al. 2011; the current study includes an additional 12 stroke subjects and 13 control subjects. Of the twenty-three stroke subjects, fourteen had right brainstem infarcts and nine had left brainstem infarcts (Supplementary Figure 1a, 2, 3). Written informed consent was obtained from all participants. Patients were scanned between two and five times over a period of 6 months. Specifically, MRIs were obtained at 7, 14, 30, 90 and 180 days after stroke onset on a 3T TimTrio Siemens using a 12-channel phase-array head coil. Fugl-Meyer assessments were performed twice for each subject at each session and averaged (Supplementary Figure 1b). The Fugl-Meyer test includes 33 tasks that assesses motor function, balance, sensation, and joint function of the upper limbs (Fugl-Meyer et al. 1975). Each task was rated on a scale of 0 to 2 (0 indicates the subject was unable to perform the task, 1 indicates the subject could partially perform the task, and 2 indicates the subject was able to perform the task). The total sum of the 33 scores was then normalized to a score between 0 and 100, where 100 represents the best possible performance across all 33 tasks. Anatomical images were acquired using a sagittal MP-RAGE three-dimensional T1-weighted sequence (TR, 1600ms; TE 2.15ms; flip angle, 9°, 1.0 mm isotropic voxels, FOV 256 x 256). Each MRI session involved between two and four runs of task-free

fMRI at 6 minutes each. Subjects were instructed to stay awake with their eyes open; no other task instruction was provided. Images were acquired using the gradient-echo echo-planar pulse sequence (TR, 3000ms; TE, 30ms; flip angle, 90°, 3 mm isotropic voxels). Anatomical MRI, lesion masks and fMRI data were processed as described below and in (Olafson et al. 2021).

Anatomical MRI processing

Preprocessing of the longitudinal anatomical MRIs included affine registration of each subject's T1 scans to the baseline T1 scan, collapsing co-registered files to an average T1 and creation of a skull-stripped brain mask followed by manual editing and binarization of the hand-edited mask. The brain mask was then transformed back to each of the follow-up T1s in native space using the inverse registration acquired from the first step. This was followed by bias field correction of all the T1 scans, transformation of native-space bias field-corrected data back to baseline space, and the creation of an average bias field-corrected scan for each subject. Stroke lesion masks were hand-drawn on these transformed T1 scans by ADB and JEB. Structural normalization was performed with the ANTs toolbox (Avants et al. 2011).

Functional MRI processing

Preprocessing of the longitudinal functional MRIs was performed using the CONN toolbox (Whitfield-Gabrieli and Nieto-Castanon 2012), including functional realignment of volumes to the baseline volume, slice timing correction

for alternating acquisition, segmentation and normalization, and smoothing with a 4 mm FWHM kernel. This was followed by a denoising protocol (CompCor) (Behzadi et al. 2007) which regressed out the cerebrospinal fluid and white matter signal, as well as 24 realignment parameters (added first-order derivatives and quadratic effects). Temporal band-pass filtering (0.008 - 0.09 Hz), despiking and global signal removal regression were also performed. The first four frames of each BOLD run were removed. Frame censoring was applied to scans with a framewise displacement threshold of 0.5 mm along with its preceding scan (Power et al. 2012b). Regional time series were acquired by parcellating the scans into 268 non-overlapping brain regions using a functional atlas derived from healthy controls (Shen et al. 2013) and averaging the time course of all voxels within a given region. Voxels identified as lesioned were excluded from regional time series calculations. The first 200 volumes from each subject's fMRI were used for subsequent analyses to ensure equal contribution of each scan to the brain state clustering (see below for details). Finally, each of 268 regions was assigned to one of 8 functional networks, identified by (Finn et al. 2015) using spectral clustering in healthy subjects (Supplementary Figure 4) named as follows: medial frontal network, frontoparietal network, default mode network, subcortical/cerebellum network, motor network, visual I network, visual II network, and the visual association network. These networks reflect collections of brain regions whose temporal signals are homogeneous at rest (i.e., the activity of regions within each network is similar over time) in a healthy population, and are referred to as canonical networks due to their repeated observation in resting-state data.

Dynamic brain states and their metrics

Following Cornblath et al. (2020), all subjects' regional fMRI time series were concatenated, producing an $n \times p$ matrix where $n = 47$ subjects * 200 TRs * 2-5 sessions and $p = 268$ brain regions). This matrix was z-scored along columns such that each brain region had a mean of 0 and a standard deviation of 1. K-means clustering was then applied to identify clusters of brain activation patterns, or states (Figure 2.1a). Pearson correlation was used as the cluster distance metric and clustering was repeated 50 times with different random initializations before choosing the solution with the best separation of the data (minimum sum of point-to-centroid distances, summed over all k clusters). To determine the optimal number of clusters and evaluate the quality of clustering, we performed several analyses (Supplementary Figure 5). First, we plotted the variance explained by clustering (between-cluster variance divided by the sum of between-cluster and within-cluster variance) for $k = 2$ to 12 and identified the curve's elbow at $k = 4$ as a potential optimal number of clusters. We also plotted the distortion curve, which is the average distance from each point to its centroid and again determined via elbow criteria an optimal cluster number of 4. We then plotted silhouette coefficients for $k = 4$ to assess if there was evidence of misassignment of any of the points. To further assess the stability of clustering and ensure our partitions were reliable at $k = 4$, we repeated the above clustering process 50 times and compared the adjusted mutual information (AMI) between each of the 50 results. The partition which shared the greatest total AMI with all other partitions was selected as the final cluster assignment. The centroids of each state (cluster) were calculated by taking the mean of all TRs assigned to that state in regional activation space (Cornblath et al. 2020). Following Cornblath et al., dominant networks in each state were determined by

calculating the cosine similarity between each of 8 networks and each centroid. High and low amplitude network-level activations were assessed separately by taking the cosine similarity of the positive and negative parts of the centroid (and zeroing out values with the opposite sign), respectively.

We performed several analyses to assess the robustness of our results under different conditions. First, we repeated the entire clustering process using two other brain atlases of varying resolutions: the group average FreeSurfer Desikan-Killany atlas with additional cerebellum and subcortical regions (86 regions) (Desikan et al. 2006) and the CC400 atlas (400 regions) (Craddock et al. 2012). Finally, we performed the clustering after combining stroke and control data together because we were interested in determining differences in shared activation states across both groups. However, it may be possible that stroke and control subjects occupy distinct states that can only be observed by clustering stroke and control subjects separately. Therefore, we repeated the clustering on the stroke and control subject data separately to determine if there were any differences in the resulting states compared to those obtained with the combined data.

FO, DT, AR and TPs were calculated separately for each of the 5 sessions (1 week, 2 weeks, 1 month, 3 months, and 6 months post baseline or stroke) and the average FO/DT/AR/TPs for each subject was obtained by taking the mean across their longitudinal sessions. State dynamics metrics were compared between groups using unpaired two-tailed t-tests and corrected for multiple comparisons using Benjamini-Hochberg (BH) and false discovery rate (FDR) of 0.05 (Benjamini and Hochberg 1995).

Assessment of corticospinal tract integrity

The probabilistic Tang brainstem atlas (Tang et al. 2018) was used to define left and right binary CST masks in 2mm MNI space by voxel-wise thresholding at 50%. The Dice overlap between the left and right CST masks and the binarized lesion mask was calculated for each subject and lesions were visualized to verify intersection with the CST (Supplementary Figure 2 and 3). In one subject (SUB13), Dice overlap with CSTs were low; however, upon visualization the lesion appeared to impact CST ventral to the atlas, i.e. in the spinal cord. This was confirmed by assessing the lesion's overlap with a spinal cord atlas (Supplementary Figure 12) using the Spinal Cord Toolbox (De Leener et al. 2017). In total, 21/23 subjects had CST damage and 10/23 subjects had damage to their dominant-hand CST, but only 9/23 had motor assessment data at the 3- and/or 6-month time points. Of the 9 subjects with dominant CST damage and motor scores, 7/23 were right-handed and either had left CST damage superior to decussation or right spinal cord CST damage inferior to decussation, 1/23 was left-handed with bilateral damage, and 1/23 was left-handed with right CST damage (Supplementary Table 1).

Relating FPN^+ state metrics to chronic motor outcomes

We were interested in determining whether FPN^+ state metrics related to longer-term (chronic) motor performance outcomes specifically in subjects with dominant hemisphere CST damage. To assess the interaction effect of hand dominance on the relationship between the frontoparietal state parameters (FO

and DT) over time and Fugl-Meyer (FM) scores over time, two linear models were constructed:

$$\Delta FM_{chronic} \sim CST_D + \Delta DT_{chronic}^{FPPN^+} + CST_D * \Delta DT_{chronic}^{FPPN^+} + \beta \quad (2.1)$$

$$\Delta FM_{chronic} \sim CST_D + \Delta FO_{chronic}^{FPPN^+} + CST_D * \Delta FO_{chronic}^{FPPN^+} + \beta \quad (2.2)$$

Where:

$$\Delta FM_{chronic} = FM_{chronic} - FM_{baseline} \quad (2.3)$$

$$\Delta DT_{chronic}^{FPPN^+} = DT_{chronic}^{FPPN^+} - DT_{baseline}^{FPPN^+} \quad (2.4)$$

$$\Delta FO_{chronic}^{FPPN^+} = FO_{chronic}^{FPPN^+} - FO_{baseline}^{FPPN^+} \quad (2.5)$$

and CST_D is a binary variable indicating whether the subject's dominant-hand CST had non-zero Dice overlap with the lesion. $FM_{baseline}$ was set to the earliest FM score available for each subject, which was the FM score at 1 week post-stroke for most of the subjects. For two subjects (SUB22 and SUB23), 1 week FM scores were not available; the baseline FM scores for these subjects

was estimated by their oldest FM score (2 weeks and 1 month, respectively). $FM_{chronic}$ was set to the most recent chronic FM score (i.e. at 3 or 6 months after stroke, whichever is later). Only one subject (SUB6) had a FM score at 3-months post-stroke but not 6-months post stroke. Two subjects (SUB12 and SUB20) were excluded from the model entirely as they did not have any FM scores or imaging data beyond 1 month and 2 weeks, respectively. The models were constructed using only the FPN^+ metrics that were found to have significant differences between stroke and controls at the 3 and 6 month time points. P-values obtained for each predictor across all models were corrected for multiple comparisons using BH-FDR and a threshold of 0.05.

Effect of proportional recovery on observed relationships

We were interested in determining whether relationships observed in the above model were driven by the correlation (if any) between DT/FO in FPN^+ and baseline FM scores in subjects with dominant-hand CST damage. Because most subjects obtained proportional recovery or greater, i.e. their final impairment was $\geq 70\%$ of their initial impairment (Kundert et al. 2019), their 1-week FM scores were strongly correlated with 3- and 6-month FM scores (a phenomenon called the ceiling effect, see Hope et al. 2019). Therefore, it is possible that relationships between ΔFM and $\Delta FO/DT^{FPN^+}$ observed in the linear model could be driven by an underlying relationship between baseline FM scores and $\Delta FO/DT^{FPN^+}$. To explore this possibility, for those FPN^+ metrics whose change had a significant correlation with baseline FM (which were chronic ΔDT^{FPN^+} and ΔFO^{FPN^+}), we performed permutation testing to obtain the null distribution of correlations between ΔFM and $\Delta FO/DT^{FPN^+}$, assuming patients obtain only proportional

recovery (PR). $FM_{baseline}$, $FO/DT_{baseline}^{FPN^+}$ and $FO/DT_{chronic}^{FPN^+}$ were fixed to their actual observed values, but $FM_{chronic}^{PR}$ was randomly generated by simulating scores according to the proportional recovery rule as in Kundert et al. 2019. Specifically, each subject's FM scores ($FM_{chronic}^{PR}$) were set to 70% of their initial impairment ($100 - FM_{baseline}$) with a noise term $\epsilon \sim N(0, 3)$:

$$FM_{chronic}^{PR} = 0.7 * (100 - FM_{baseline}) + \epsilon \quad (2.6)$$

The p-value for the correlation between the observed ΔFM and $\Delta FO/DT^{FPN^+}$ and was then calculated by calculating the proportion of times the null correlation exceeded the true correlation (Supplementary Figure 14c,d). If that p-value is significant, then we can be more confident that $\Delta FO/DT^{FPN^+}$ is correlated with the change in FM above and beyond baseline FM and the expected proportional recovery.

Comparison of fractional occupancy and functional connectivity

Finally, we wanted to understand how differences in state dynamics between controls and stroke subjects could translate to differences in FC between the two groups. We hypothesize that individuals with more TRs (higher FO) in a brain state with high co-activation of two networks will result in larger positive FC between those networks, while more TRs (higher FO) in a brain state with large activations in opposite directions (contra-activation) of two networks will result in a more negative FC between those networks (Supplementary Figure 15). We tested this hypothesis for our brain state of interest, FPN^+ , in the following way. First, we identified the pairs of networks that were highly co-activated/contra-

activated during FPN^+ , which was defined as having an absolute value cosine similarity with the centroid of FPN^+ of greater than 0.2 (chosen heuristically as the threshold separating networks active vs. not active during a given state). We only analyzed the networks with larger magnitude co-activations/contra-activations since the networks with activity closer to zero in the FPN^+ state are not likely to be influenced by changes in FO of this state. We first calculated the functional connectivity as the Pearson's correlation between each pair of 268 regions and performed a Fisher's r-to-z transformation of the FC weights. We then averaged the FC values between regions belonging to each pair of networks to produce a network-level FC (i.e., the average FC within each of 8 predefined networks, including the frontoparietal network). We correlated each subject's FO in the FPN^+ state with the FC between each pair of networks determined to be highly co-activated/contra-activated in the FPN^+ state. In an analysis inspired by Baker et al. 2014, we further demonstrated that temporal fluctuations in FO^{FPN^+} over segments of the scan are related to sliding window FC in nodes of the frontoparietal network. We first identified regions with high z-score BOLD signal in the FPN^+ centroid (greater than 0.4), and, for those regions, calculated their sliding-window FC and FO^{FPN^+} using the same window and overlap (window size = 45 seconds, overlap = 3 seconds). We then correlated these two values over the entire fMRI scan for each individual. To ensure any observed relationship was not driven by global BOLD fluctuations, we recalculated this correlation using 100 randomly selected regions' dynamic FC as a null comparison.

Statistics and reproducibility

We calculated statistics comparing brain dynamic parameters between stroke and control groups. Where stated, comparisons were corrected for multiple comparisons to reduce type I error. The clustering was repeated 50 separate times to ensure the the final solution was not in large disagreement with other possible solutions. We replicated the main analyses with k=5 brain states and found a general agreement between the results obtained with k=4. Code for the analyses in this manuscript have been made publicly available.

Data availability

Data is not publicly available due to privacy issues regarding clinical data. Raw data to generate Figures 3 and 6e can be found in the Supplementary Data. All other data can be made available upon request to the corresponding authors on the condition that a formal data sharing agreement is made.

Code availability

The code to replicate this analysis is available on GitHub: <https://github.com/emilyolafson/brainstates> and Zenodo (Olafson 2022).

2.3 Results

2.4 Discussion

2.5 Conclusions

CHAPTER 3

CHAPTER 3

3.1 Introduction

Stroke is a leading cause of long-term disability worldwide (Katan and Luft 2018). Motor impairments are the most common deficit after stroke, and up to 50 percent of stroke survivors will have lasting hemiparesis (Kelly-Hayes et al. 2003). Providing accurate predictions of long-term motor outcomes is an ongoing goal of stroke research, as predictions based on acute clinical information can inform individualized rehabilitation strategies and can guide patient selection in clinical trials (Bonkhoff and Grefkes 2022; Boyd et al. 2017). Biomarkers derived from routinely-collected structural neuroimaging data that reflect lesion location with respect to critical white matter tracts have been related to motor outcomes (Tozlu et al. 2020; Kuceyeski et al. 2016; Griffis et al. 2019; Salvalaggio et al. 2020; Bowren et al. 2022). However, there is no consensus on how to optimally model lesion-induced disruption of structural connections to produce generalizable predictions of chronic motor deficits.

The most well-studied biomarker is the corticospinal tract (CST) lesion load, or the proportion of voxels in the ipsilesional corticospinal tract (typically originating from primary motor cortex, M1) that intersect with the lesion (Zhu et al. 2010; Feng et al. 2015; Findlater et al. 2019; Lam et al. 2018; Pineiro et al. 2000). M1-CST lesion load has been related to motor deficits in the acute and chronic phase of stroke (Boyd et al. 2017; Kim and Winstein 2017), but M1-CST damage in itself is unlikely to capture enough variance in lesion data to explain motor deficits in patients with a wide range of lesion topographies (Park, Kou, and

Ward 2016; Findlater et al. 2019). Including damage to higher order motor areas explains more variance in post-stroke motor outcomes than damage to M1 alone (Ito et al. 2022; Rondina et al. 2016; Rondina, Park, and Ward 2017; Schulz et al. 2012; Park, Kou, and Ward 2016). For instance, Ito et al. 2022 use the sensorimotor tract template atlas to calculate lesion load (SMATT-LL) to several tracts originating from primary motor, premotor, somatosensory, and supplementary motor regions, and find that post-stroke motor outcomes are explained best by damage to fibers originating from M1 and from ventral premotor cortex.

These somatomotor tracts were selected a priori on the basis of their known theoretical involvement in motor function. However, in the context of prediction, where we simply wish to exploit associations between lesion data and motor deficits with the goal of optimizing out-of-sample predictive accuracy, limiting input features to predefined structures in the motor system may limit model performance. Non-causal associations between damage and deficits exist in stroke because the distribution of lesions is influenced by vascular anatomy, and regions that are not related to a deficit may be consistently damaged alongside a critical region in a way that makes the two regions statistically indistinguishable (Mah et al. 2014). In other words, we may want to discover useful lesion-deficit associations in a data-driven way instead of assuming that theory-based structure-function relationships will have maximal predictive value (Bzdok, Engemann, and Thirion 2020; Bonkhoff and Grefkes 2022).

Lesion-behaviour mapping (LBM) is a technique used to discover neural correlates of a behavioural deficit that involves associating voxelwise lesion damage with the presence or degree of a deficit (Bates et al. 2003; Karnath et al. 2020). Maps of association can be derived from multivariate models that relate

deficits to patterns of damage across multiple voxels simultaneously (Ivanova et al. 2021; Karnath et al. 2020; Zhang et al. 2014; Sperber, Wiesen, and Karnath 2019). These multivariate models generate maps using one of two statistical frameworks: inference or prediction (Sperber, Griffis, and Kasties 2022; Bzdok, Engemann, and Thirion 2020). In an inference framework, these maps consist of voxels in which damage is significantly associated with a deficit. While inferential methods have been used successfully to evaluate hypotheses and generate explainable results, statistical significance does not necessarily imply good generalization performance (Bzdok, Engemann, and Thirion 2020). On the other hand, in a prediction framework, lesion-behaviour maps are comprised of patterns of voxels in which damage is predictive of impairment in new subjects (Bowren et al. 2022; Mah et al. 2014; Rondina, Park, and Ward 2017; Sperber 2020). Lesion-behaviour maps derived from a predictive framework may be more suitable as input features to predictive models, given that those maps to some degree already contain features in which damage predicts impairment in new subjects (Zhang et al. 2014). In light of the importance of the brain's structural networks in motor function, Bowren et al. 2022 perform multivariate lesion-behaviour mapping to identify patterns of voxels in which damage predicts motor impairments. Then, they identify the structural connections that pass through the peak voxels identified with predictive LBM, thus placing the findings within the context of a broader disrupted structural network. Damage to those structural connections (lesion load on structural lesion network maps, sLNM-LL) as features in predictive models. These features are derived in a data-driven way from predictive multivariate lesion-behaviour mapping and have already shown promising predictive potential (Bowren et al. 2022), but have yet to be formally cross-validated in an independent dataset.

Multivariate lesion-behaviour analyses (including Bowren et al. 2022) traditionally identify combinations of voxels in which damage is associated with a deficit. This high-dimensional, voxelwise lesion representation may hamper predictive models: when no patients have lesions in a given voxel, associations between damage and impairment cannot be detected (Kimbberg, Branch Coslett, and Schwartz 2007; Rorden, Fridriksson, and Karnath 2009; Sperber 2020; Griffis et al. 2019). Instead of relating voxelwise lesion damage to deficits, one can first identify the white matter tracts that pass through the lesion using structural connectomes from healthy subjects as a reference, a technique known as structural disconnection-behaviour mapping (Kuceyeski et al. 2013; Kuceyeski et al. 2016; Salvalaggio et al. 2020; Griffis et al. 2019; Sperber, Griffis, and Kasties 2022). This is in effect a dimensionality reduction of voxelwise lesion data that can identify, for instance, damage to the same white matter tract by non-overlapping lesions. Projecting voxelwise lesion data into lower-dimensional structural disconnection space may be a biologically-relevant way to preserve variance in lesion-deficit relationships while improving statistical power. Using the Network Modification tool (Kuceyeski et al. 2013), the amount of lesion-induced structural disconnection for each gray matter region in the brain can be estimated. Similar to recent approaches in multivariate lesion behaviour mapping (Kasties, Karnath, and Sperber 2021), feature selection can be employed to identify subsets of regions that are relevant for predicting chronic motor scores in new subjects. Selecting features in a data-driven way and estimating the performance of resulting models often requires many subjects; with the rising availability of large stroke imaging databases (Liew et al. 2020), multivariate predictive models can be trained and evaluated in the same study.

In this paper, we compare the out-of-sample predictive performance of several lesion damage metrics using a large, diverse stroke imaging dataset ($N = 789$). First, we assess the predictive performance of theory-based biomarkers, including M1-CST-LL and SMATT-LL, that reflect damage to known somato-motor white matter tracts. We then evaluate the performance of data-driven biomarkers: sLNM-LL, which reflects damage to white matter tracts associated with peak voxels from multivariate predictive lesion-behaviour mapping, and ChaCo scores, which compress voxelwise data into regional structural disconnectivity measures. In this final model, we evaluate the use of feature selection to identify regions in which structural disconnectivity is predictive of chronic motor scores.

Our primary objective was to determine the relative performance of different biomarkers for predicting chronic motor scores, with the hypothesis that data-driven models would have superior prediction performance compared to theory-based biomarkers based in the motor system. As a secondary objective, we assessed whether predictive performance could be improved by incorporating demographic information and by combining predictions from several different biomarkers using ensemble models.

3.2 Methods

3.2.1 Sample demographics

A subset of cross-sectional data from the Enhancing Neuroimaging Genomics through Meta Analysis (ENIGMA) Stroke Recovery Working Group database

(available as of 10 Sept. 2021) was used in the study. Details of the ENIGMA Stroke Recovery procedures and methods are available in (Liew et al. 2020). The data originated from 22 research studies (sites) (Table ??). Informed consent was obtained from all subjects, and data were collected in compliance with each institution's local ethical review boards and in accordance with the Declaration of Helsinki.

ENIGMA Stroke Recovery participants with the following data were included: (1) high-resolution (1-mm isotropic) T1-weighted brain MRI (T1w) acquired with a 3T MRI scanner; (2) information about time since stroke at time of imaging (3) age, (4), sex, and (5) measurem of motor function from one of the following assessments: Fugl Meyer Assessment of Upper Extremities (FMA-UE), a performance-based measure of paretic upper extremity impairment (Gladstone, Danells, and Black 2002); the Action Research Arm test (ARAT) which tests arm function through assessment of the timing and difficulty of motor task completion (Yozbatiran, Der-Yeghiaian, and Cramer 2008); the Barthel index, which measures the extent to which a person can function independently and has mobility in their activities of daily living (Sulter, Steen, and De Keyser 1999); National Institutes of Health Stroke Score (NIHSS), a broad measure of stroke severity that includes assessment of non-motor and motor functions (Lyden 2017). Motor scores were normalized to the range [0, 1] by dividing by the raw score by the maximum possible score on the assessment. For a majority of the chronic stroke subjects (76%), motor deficits are normalized FMA-UE scores, whereas normalized FMA-UE scores were available for only 12% of the acute stroke subjects (for full breakdown of type of test used for each site in the dataset, see Supplementary Table ??). behavioural data were collected within approximately 72 hours of the MRI. Subjects were considered in the chronic phase of stroke if their time since

stroke at the time of assessment was greater than 180 days, and considered in the acute phase if their time since stroke at the time of assessment was less than 180 days (Bernhardt et al. 2017). Subjects with cortical and subcortical lesions were included in the study; lesions were not flipped (see Supplementary Figure ?? for lesion distribution in MNI space).

Table 3.1: Demographic information of the acute subjects in the ENIGMA dataset, broken down by chronicity (acute/chronic) and by site within each chronicity group. Total sample size (N), number of females (F) and males (M), and information about age (years), normalized motor scores, time since stroke at the time of assessment (months), and lesion volume (cm^3). IQR, interquartile range

Site ID	Total N. (F/M)	Median age in years (IQR)	Median motor score (IQR)	Median time since stroke (IQR)	Median lesion vol, cm^3 (IQR)
Acute					
r005	1 (0/1)	50.0 (0.0)	0.29 (0.00)	5.1 (0.0)	1.7 (0.0)
r009	50 (13/37)	70.0 (18.5)	1.00 (0.05)	0.2 (0.1)	1.7 (7.0)
r025	9 (4/5)	70.0 (19.0)	1.00 (0.09)	3.0 (1.0)	0.5 (1.4)
r028	1 (0/1)	63.0 (0.0)	0.74 (0.00)	5.5 (0.0)	23.9 (0.0)
r031	36 (10/26)	58.5 (13.2)	0.52 (0.38)	4.5 (1.7)	10.8 (38.8)
r038	72 (30/42)	66.5 (21.2)	0.78 (0.66)	2.9 (2.3)	11.5 (41.6)
r040	57 (32/25)	64.0 (22.0)	0.40 (0.50)	1.8 (1.5)	14.7 (58.6)
r047	2 (1/1)	71.0 (2.0)	0.59 (0.26)	4.4 (0.2)	23.8 (19.2)
r049	21 (12/9)	65.0 (16.0)	0.95 (0.00)	0.0 (0.0)	1.3 (2.2)
r050	14 (7/7)	68.0 (16.8)	0.92 (0.10)	0.0 (0.0)	0.3 (0.4)
r053	52 (20/32)	63.5 (20.5)	0.92 (0.17)	3.0 (3.0)	13.5 (28.3)
r054	12 (5/7)	65.5 (11.8)	0.67 (0.83)	0.4 (0.2)	4.1 (14.1)
Chronic					
r001	39 (10/29)	61.0 (17.0)	0.65 (0.23)	23.5 (40.0)	6.3 (18.1)
r002	12 (6/6)	69.5 (11.5)	0.50 (0.41)	73.2 (51.9)	28.2 (31.7)
r003	15 (6/9)	61.0 (16.5)	0.24 (0.20)	48.8 (67.6)	20.3 (76.9)
r004	19 (7/12)	44.0 (14.5)	0.17 (0.16)	50.4 (81.9)	36.9 (44.3)
r005	27 (12/15)	66.0 (16.5)	0.79 (0.45)	31.4 (27.8)	1.6 (40.3)
r009	60 (17/43)	71.0 (7.2)	0.96 (0.12)	27.4 (9.3)	1.4 (4.7)
r025	16 (3/13)	64.5 (13.2)	0.98 (0.58)	14.2 (10.2)	5.9 (14.3)
r027	28 (8/20)	57.0 (10.2)	0.30 (0.16)	19.3 (24.7)	12.3 (62.1)
r028	21 (6/15)	63.0 (9.0)	0.82 (0.24)	26.5 (37.5)	5.2 (41.3)
r031	1 (0/1)	52.0 (0.0)	0.68 (0.00)	6.1 (0.0)	1.5 (0.0)
r034	15 (6/9)	58.4 (11.1)	0.82 (0.20)	61.3 (68.3)	6.7 (35.0)
r035	15 (6/9)	64.0 (18.0)	0.64 (0.52)	33.5 (22.9)	3.9 (31.6)
r038	18 (7/11)	67.0 (10.0)	1.00 (0.12)	15.1 (10.1)	2.0 (1.6)
r040	14 (7/7)	63.5 (9.8)	0.68 (0.47)	14.1 (17.5)	8.6 (82.7)
r042	22 (11/11)	48.5 (15.5)	0.64 (0.19)	29.6 (36.4)	14.1 (49.5)
r044	4 (0/4)	68.0 (9.2)	0.52 (0.25)	43.7 (52.9)	23.7 (67.0)
r045	4 (1/3)	62.0 (5.2)	0.49 (0.24)	96.1 (59.0)	8.0 (6.7)
r046	11 (3/8)	62.0 (10.5)	0.50 (0.29)	86.3 (83.4)	4.6 (19.8)
r047	44 (14/30)	65.5 (12.0)	0.65 (0.44)	38.1 (53.7)	12.7 (41.3)
r048	43 (16/27)	68.0 (12.5)	0.79 (0.44)	46.2 (49.8)	7.9 (43.4)

Table 3.1: (continued)

r052	32 (12/20)	63.0 (13.5)	0.41 (0.09)	39.1 (42.2)	7.0 (51.5)
All					
	789 (293/496)	64.0 (18.0)	0.7 (0.5)	12.2 (0.2)	6.5 (32.5)

3.2.2 General overview

We built several models to predict chronic motor scores from imaging data and minimal clinical information. Each model uses lesion-derived information as input to predict normalized motor scores in chronic stroke subjects. We compared several different features that reflect different aspects of lesion damage. These features include: lesion load to ipsilesional M1 (1 feature), lesion load of higher order motor tracts (6 features for ipsilesional tracts, 12 features in left and right hemisphere tracts together) structural lesion-behaviour mapping components (5 features based on Bowren et al. 2022), and measures of structural disconnection reflecting damage to gray matter regions across the entire brain (2 atlases assessed with 86 or 268 features; fewer with feature selection). We assessed whether data-driven feature selection improved performance for models using whole-brain measures of structural disconnection. Nested cross-validation was performed for all measures to train models and assess performance on unseen data. Additionally, we evaluated whether including acute subjects in the training set (but not in the test set) improved prediction of chronic deficits, with the idea that the signal in the acute data would be useful in predicting deficits in the chronic phase. We also evaluated whether adding basic clinical information (age, sex, time since stroke) with ensemble models improved performance. Finally, we

assessed whether using ensemble models to combine predictions from multiple different lesion damage metrics improved performance.

Machine learning framework

Models differed for each lesion biomarker based on the data; see below (3.3 Description of models and their inputs) for implementation details for each biomarker. In general, regression models were trained and evaluated using repeated 5-fold nested cross-validation loop. In the outer loop, the data was split into 5 training and test partitions. Using only chronic data to train the models, there were approximately 370 subjects in the training set and 92 subjects in the test set. If acute data was used in training, it was added to the training partition, such that there were 696 subjects in the training set and 92 subjects in the test set. Training data was further partitioned into training and validation sets in the inner loop, and if hyperparameters were specified in the model, they were optimized in the inner loop.

Out-of-sample performance was calculated as the average performance across 5 outer test folds. We obtained a distribution of out-of-sample performance by splitting the data into 5 train/test folds 100 times, shuffling the indices of the splits each time.

Model performance

Model performance was assessed by comparing true normalized motor scores with predicted scores. Performance was calculated with Pearson's correlation coefficient and by the explained variance score, or R^2 , which captures the percent

of variation in motor scores explained by variation in the model predictors. Two performance metrics were used in order to compare results with prior literature, which uses both.

3.2.3 Description of models and their inputs

Primary motor cortex CST lesion load (M1-CST-LL) models

The lesion load of the corticospinal tract originating from the primary motor cortex (M1-CST-LL) has been associated with motor impairment (Stinear 2017). Here, as in previous work, M1-CST-LL was calculated as the proportion of lesioned voxels intersecting with a binarized ipsilesional M1-CST template (Zhu et al. 2010). Specifically, lesion load was calculated in 1mm MNIV6 space as:

$$\text{Lesion load} = \frac{\text{Number of lesioned voxels intersecting with tract}}{\text{Number of voxels in tract}} \quad (3.1)$$

Left and right hemisphere M1-CST segmentations in MNI space were obtained from the high-resolution sensorimotor area tract template (SMATT) (Archer, Vaillancourt, and Coombes 2018). M1-CST-LL had a heavy-tailed distribution (Supplementary Figure ??A). Linear regression was used to model the relationship between ipsilesional M1-CST-LL and chronic motor scores. The weights from best-performing model in the inner loop were used to predict motor scores for new subjects in the test folds.

Sensorimotor tract lesion load (SMATT-LL) models

Sensorimotor tract segmentations were obtained from the sensorimotor area tract template (SMATT) (Archer, Vaillancourt, and Coombes 2018), a set of 12

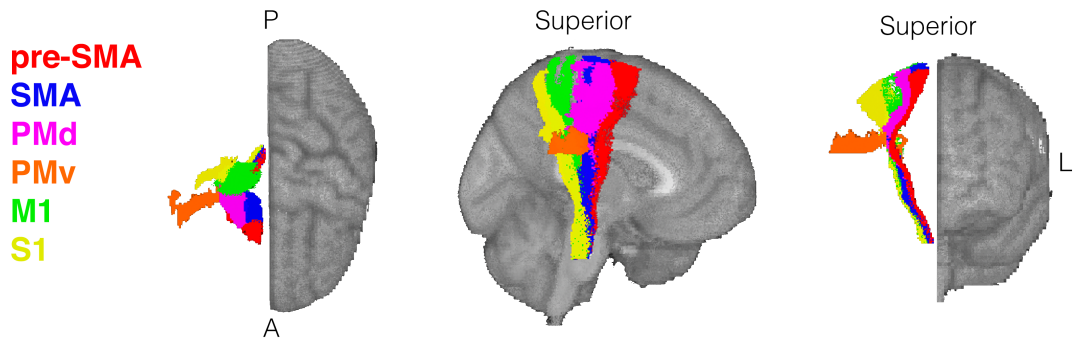


Figure 3.1: Sensorimotor tract template atlas (SMATT), displaying only right hemisphere tracts relative to an MNI template. Includes supplementary motor area (SMA), dorsal premotor cortex (PMd), ventral premotor cortex (PMv), pre-supplementary motor area (pre-SMA), primary sensory cortex (S1), and primary motor cortex (M1). Pre-SMA is the most anterior tract, S1 is the most posterior tract.

tracts derived from probabilistic tractography seeded in the left and right primary motor cortex (M1), dorsal and ventral premotor cortex (PMd and PMv, respectively), supplementary motor area (SMA), pre-supplementary motor area (pre-SMA), and primary somatosensory cortex (S1) of healthy controls (Figure ??A). Lesion load was calculated as above, for all 12 tracts, i.e., separately for left and right hemispheres, referred to as L/R SMATT-LL, and for the 6 ipsilesional tracts, referred to as Ipsilesional SMATT-LL. L/R SMATT-LL was calculated in order to assess whether preserving hemispheric information improved predictions. For subjects with brainstem, cerebellar, and/or bilateral cerebral strokes ($N=30$ chronic, $N=43$ acute), ipsilesional lesion load was calculated as the average lesion load of the left and right hemisphere tracts. Lesion loads also had a heavy-tailed distribution (Supplementary Figure ??B,C).

Ridge regression models were used to predict chronic motor deficits from ipsilesional SMATT-LL (6 features) and from L/R-SMATT-LL (12 features). Ridge regression was used to account for multicollinearity of lesion load values between tracts (Supplementary Figure ??, ??). Lesion load values were normalized (after

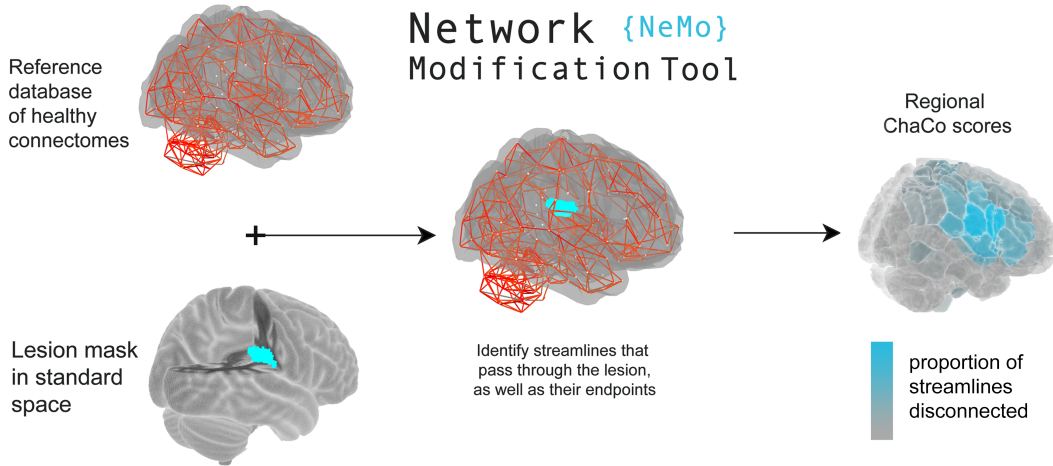


Figure 3.2: Overview of the Network Modification tool. Binary lesion masks in MNI space representing the presence of a stroke lesion (turquoise) in a given voxel are provided by the user. Each lesion mask is embedded into 420 unrelated healthy structural connectomes (separately for each healthy subject) and the regional or pairwise change in connectivity (ChaCo) scores are calculated and averaged across healthy subjects (parcellation shown here is the Shen 268-region atlas).

train/test split) by subtracting the mean across subjects and dividing by the l2-norm prior to model fitting. In the inner loop, the degree of regularization on regression coefficients (λ) was determined via grid-search, searching over 30 values ranging [10^{-2} to 10^2]. The training data was fit with the selected λ and this model was used to predict motor scores for new subjects in the test folds.

Structural lesion-network mapping (sLNM) models

Structural lesion network maps were obtained from Bowren et al. 2022. Specifically, Bowren et al. 2022 produced maps of white matter (WM) voxels in which damage predicted with Fugl-Meyer scores using sparse canonical correlations analysis (Pustina et al. 2018). Then, tractography was seeded from those peak WM voxels to identify the structural networks associated with peak areas, which produced structural lesion network maps (sLNMs). Principal components anal-

ysis of sLNMs was performed, which produced 3 principal components that correspond to 5 sLNM maps (PC1, and positive/negative weights of PC2 and PC3 split). Lesion load on each sLNM map was calculated for each subject as the sum of the voxel intensities from the principal component map that also appeared within the boundaries of a lesion mask (Supplementary Figure ??). Ridge regression models were used to predict chronic motor deficits from sLNM lesion loads (5 features). As above, lesion load values were normalized (after train/test split) by subtracting the mean across subjects and dividing by the l_2 -norm prior to model fitting. In the inner loop, the degree of regularization on regression coefficients (λ) was determined via grid-search, searching over 30 values ranging [10^{-2} to 10^2]. The training data was fit with the selected λ and this model was used to predict motor scores for new subjects in the test folds.

Regional change in connectivity (ChaCo) models

Lesion masks in $1mm^3$ MNI v6 space were processed with the Network Modification Tool (NeMo Tool) v2 pipeline (Kuceyeski et al. 2013) (<https://github.com/kjamison/nemo> for more detailed information). Given a lesion mask, the NeMo tool produces outputs that reflect the impact of the lesion on white matter tracts on the brain using healthy structural connectomes as a reference. The NeMo tool embeds a lesion mask into healthy structural connectomes, identifies all white matter streamlines that intersect with the lesion, and determines the brain regions at the endpoints of those streamlines (Figure ??B). Regional change in connectivity (ChaCo) scores, or the ratio of the number of disrupted streamlines divided by the total number of streamlines terminating in each region, were calculated for all gray matter regions (see Supplementary

Figure ??A,B for distribution of mean and standard deviation of ChaCo scores). The NeMo tool uses structural connectivity from 420 unrelated subjects from the Human Connectome Project Young Adult database. For each stroke lesion, the NeMo tool calculates regional ChaCo scores for all HCP subjects separately and then produces final regional ChaCo scores by taking the mean across HCP subjects. Structural connectivity in HCP subjects was obtained using deterministic tractography (SD stream) with dynamic seeding, with additional SIFT2 weighting for each of 5 million streamlines (Smith et al. 2015). Regional ChaCo scores from two different atlases were compared: the 86-region Desikan-Killiany Atlas (68 cortical regions + 18 subcortical regions, excluding brainstem) from FreeSurfer ("fs86" for short), which contains coarse anatomically parcellated regions (Desikan et al. 2006; Fischl et al. 2002), and the 268-region Shen atlas ("shen268" for short), which contains more fine-grained functionally parcellated cortical and subcortical regions (Shen et al. 2013).

First, the performance of ridge regression models was assessed, as described above, with regional ChaCo scores as inputs (86 features for the fs86 atlas, 268 features for the shen268 atlas). Second, a filter-based feature selection step was added to ridge regression models to obtain a subset of features that were the most useful for prediction (Guyon and Elisseeff 2003; Hall 1999; Pudjihartono et al. 2022). We mixed hyperparameter tuning and feature selection in the same step, considering the number of features as a hyperparameter itself. Features were ranked by their association with the outcome variable (p-value from univariate correlation). In the inner loop, both the amount of regularization on regression coefficients (λ) and the number of features to retain in the feature selection step (κ) were selected via grid search. The λ value was chosen by searching over 30 values ranging [10^{-2} to 10^2], and the κ value was chosen by

searching 30 values ranging from 5 to the maximum number of features possible (for fs86: 86, for shen268: 268) in base-2 steps.

Ensemble models

We tested whether models including demographic information (age, sex, and days post stroke) alongside lesion data will perform better than models with lesion data or demographic data alone (i.e., variance explained from lesion data and demographic data is not redundant). We also assessed whether models including both lesion load and ChaCo scores will perform better than models with lesion load or ChaCo scores alone. The idea of ensemble learning is to build a single prediction model by combining the strengths of a collection of simpler base models; we used ensemble models that average predictions from different damage metrics (Hastie, Friedman, and Tibshirani 2001).

Ensemble models were generated by training ChaCo-models and lesion load models separately, on the same subjects and with the same training/test/validation splits, and averaging the final predicted scores for each subject. A standard linear regression model was used to model the relationship between demographic information and motor impairment.

Model comparisons

Differences in performance between models were assessed using two-sided Mann-Whitney U tests. P-values were corrected for multiple comparisons using the Bonferroni correction.

Consistency of feature weights

The stability of the beta coefficients for the best-performing models was assessed as follows. For the 86-region ChaCo models, the average of the 86-region weight vector across 5 folds was calculated for each permutation. This represents the average beta weights of the 5 best-performing models across cross-validation splits. The distribution of the average beta coefficients of all features across 100 permutation was plotted. For the 268-region ChaCo models with feature selection, the most consistently-selected features (selected in at least 475/500 folds or 99% of folds, heuristically) were identified and the average of those features across 5 folds was calculated for each permutation. This was done because the stability of features that were not consistently selected (which effectively have a weight of 0 in the model) was not relevant. The distribution of the average beta coefficients of consistently-selected features across 100 permutations was plotted.

Code availability

All analysis scripts that generated the results of the present study are readily accessible and open for reuse (https://github.com/emilyolafson/lesion_predictions). The script can be easily modified to predict any outcome score from ChaCo scores/lesion load data.

APPENDIX A
SUPPLEMENTARY MATERIAL FOR CHAPTER 1

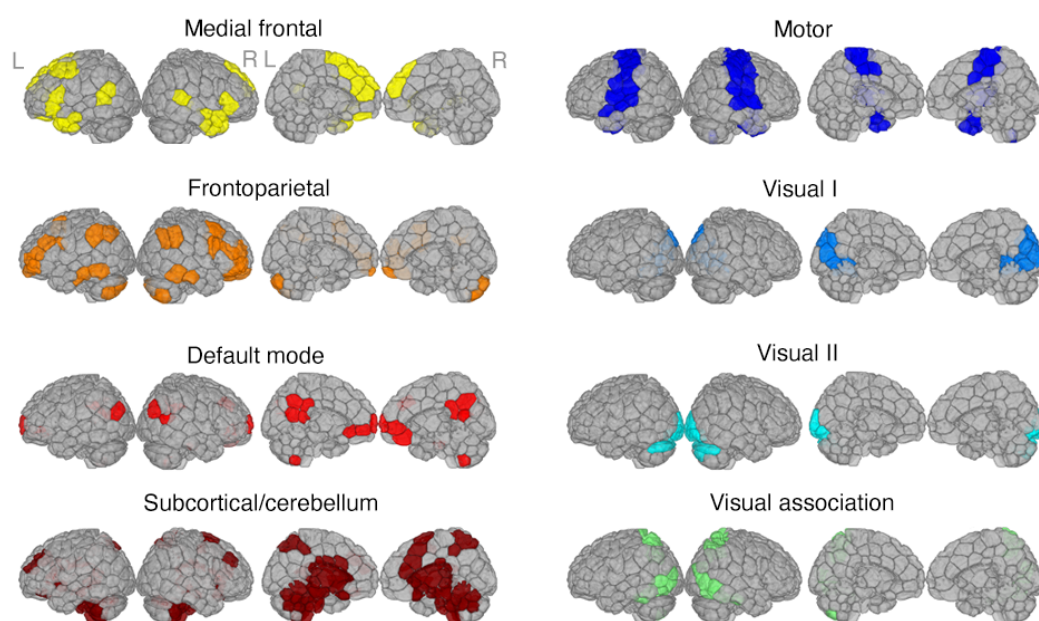


Figure A.1: Functional network visualizations.

8 functional networks identified by (Finn et al. 2015) by clustering healthy functional connectivity matrices.

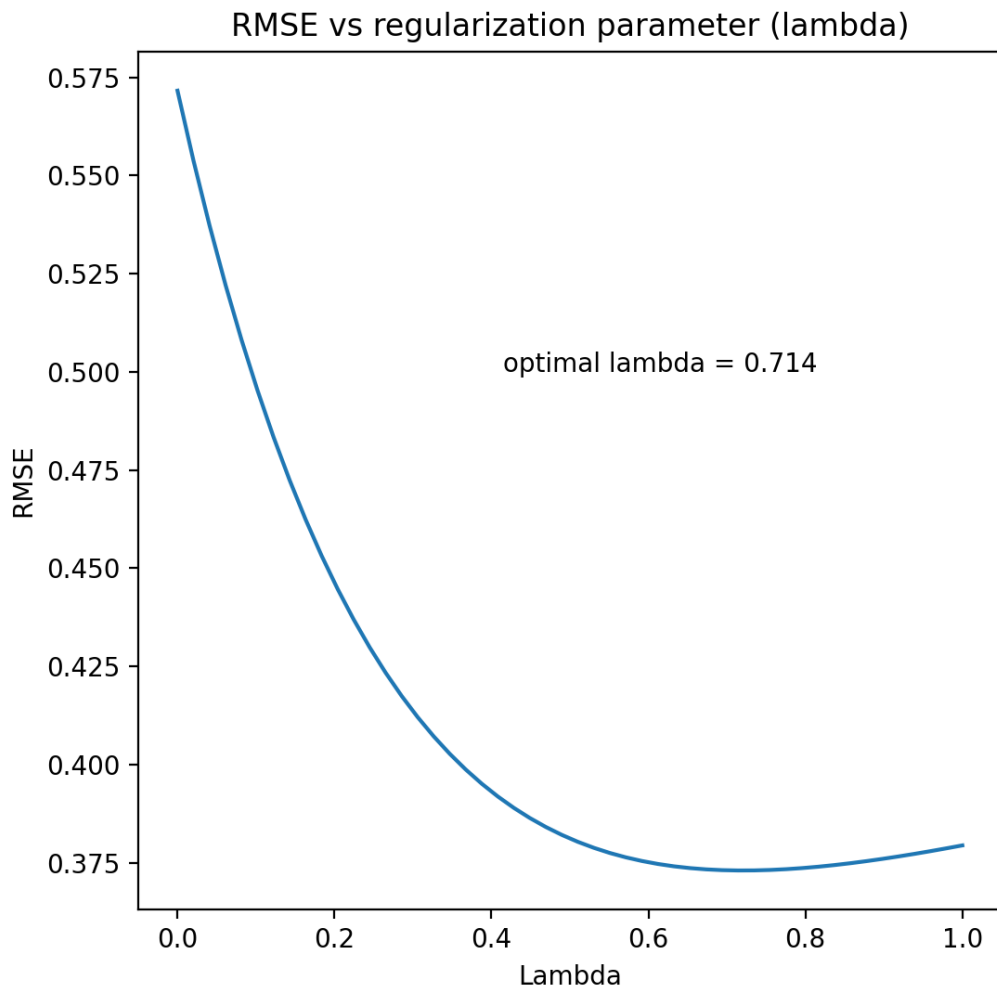


Figure A.2: Results of optimization procedure to choose the best regularization parameter, lambda (λ).

The lambda that is chosen is the one that minimizes the root mean squared error of the Frobenius norm of the difference in regularized subject precision matrices P_i^{reg} and the group average unregularized precision matrix P_{avg} , which was found to be $\lambda = 0.71$.

Figure A.3: Functional connectivity (node strength) differences between stroke and control subjects.

Significant differences and node strength (for a single node, node strength is the sum of connectivity weights to all other nodes), assessed with mass-univariate t-tests at each node and corrected with Benjamini-Hochberg FDR correction. Left hemisphere is the leftmost brain; right hemisphere is the rightmost brain. Top row shows the lateral view, bottom row shows a medial view.

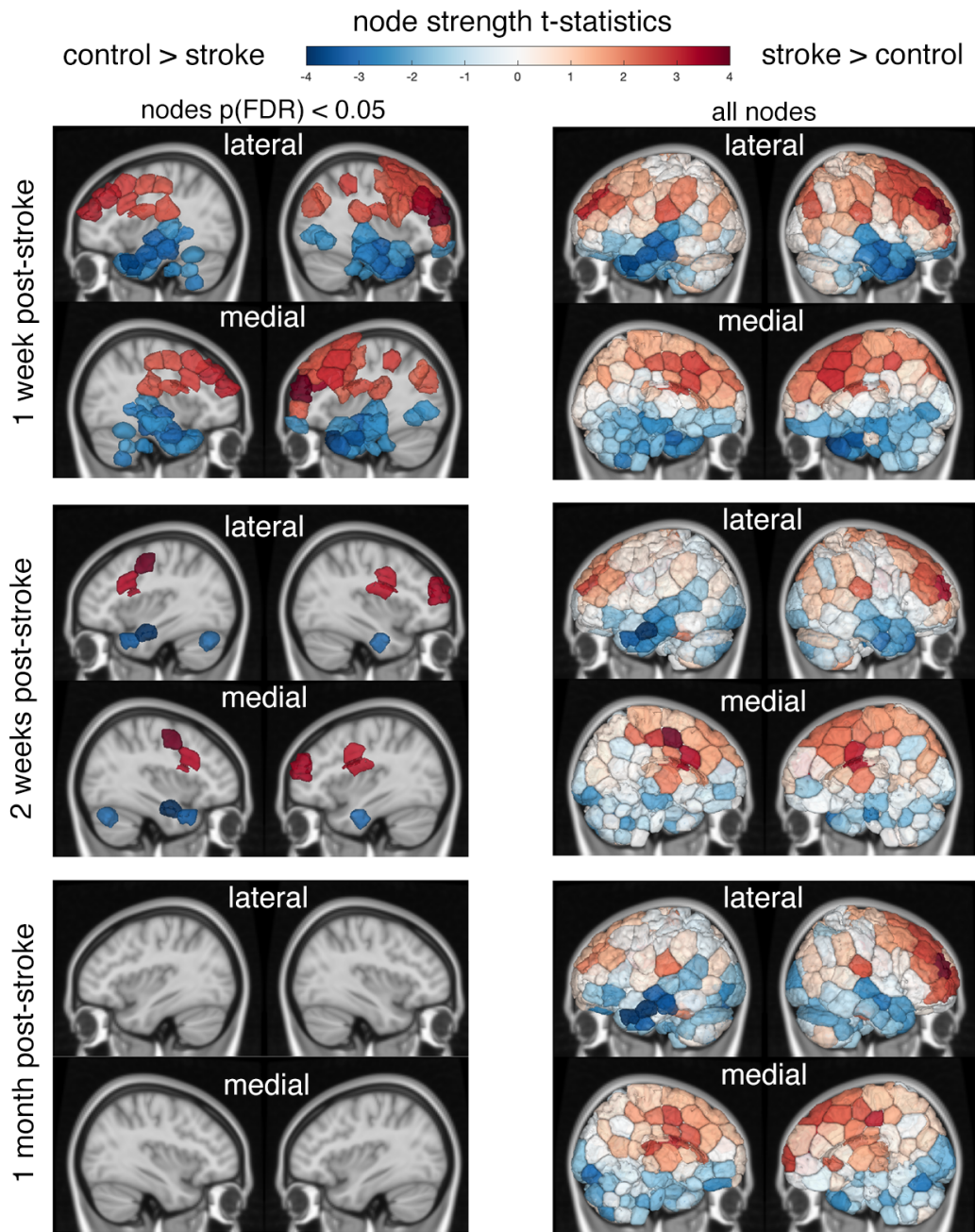


Figure A.3 (Continued)

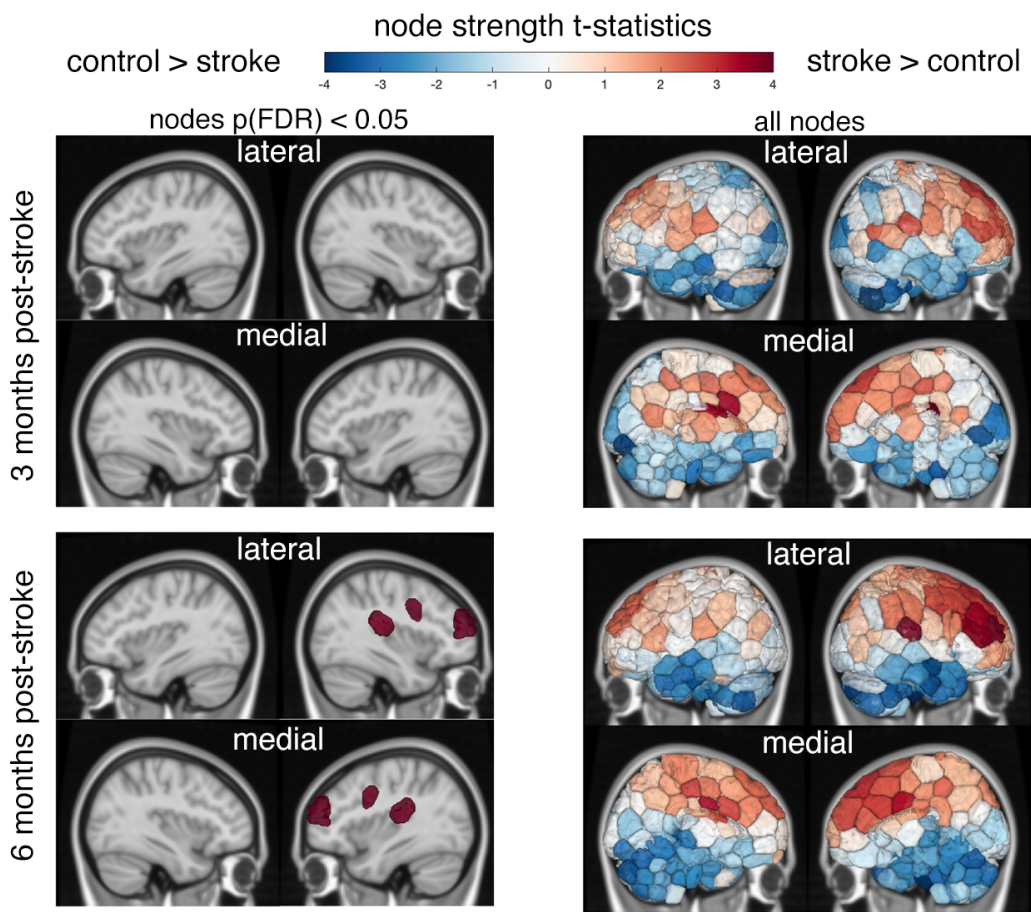


Figure A.3 (Continued)

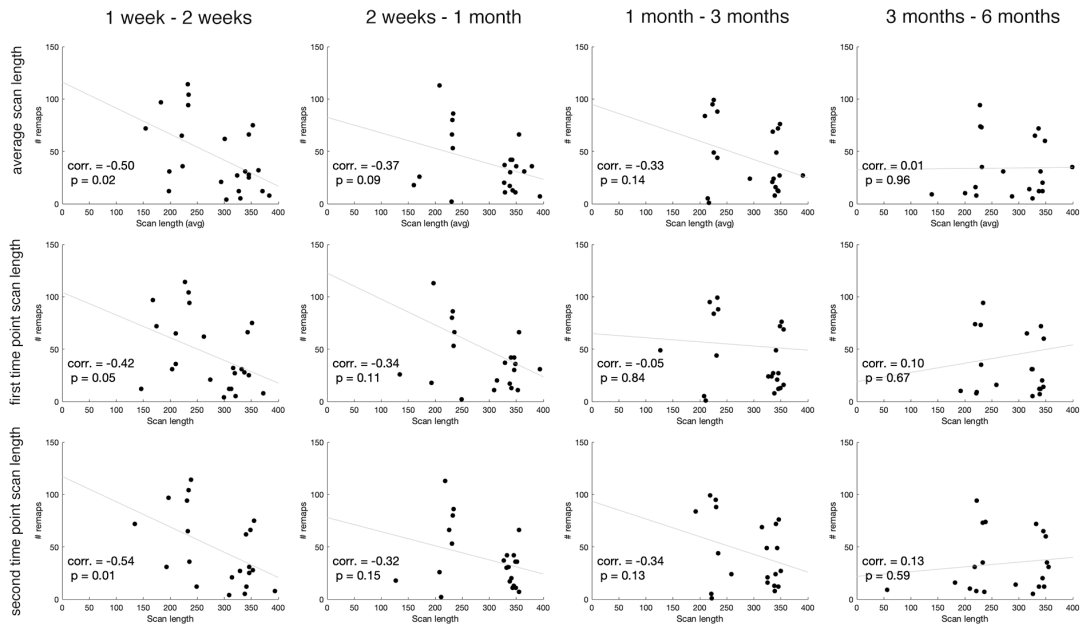


Figure A.4: Correlation between scan length (number of TRs after motion scrubbing) and remapping.

Top row: correlation between the total number of remaps observed between time points (column) and the average scan length of the two time points. Middle row: correlation between the total number of remaps observed between the number of remaps and the scan length of the first time point (chronologically). Bottom row: correlation between the total number of remaps observed between the number of remaps and the scan length of the second time point (chronologically)..

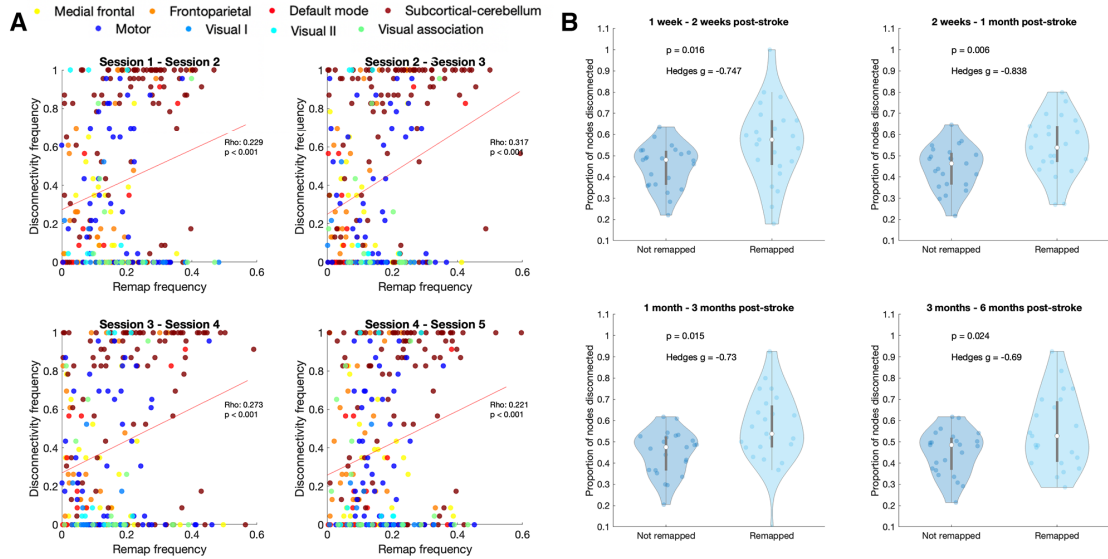


Figure A.5: Relationship between disconnection frequency and remapping frequency.

Remapping preferentially occurs in regions with greater structural connectivity disruption. **A.** Correlations between average ChaCo scores and regional remap frequencies across all 23 stroke subjects. Regions are colored by network assignment. **B.** Nodes that remap have a higher proportion of disconnected nodes than nodes that do not remap, for all time points.

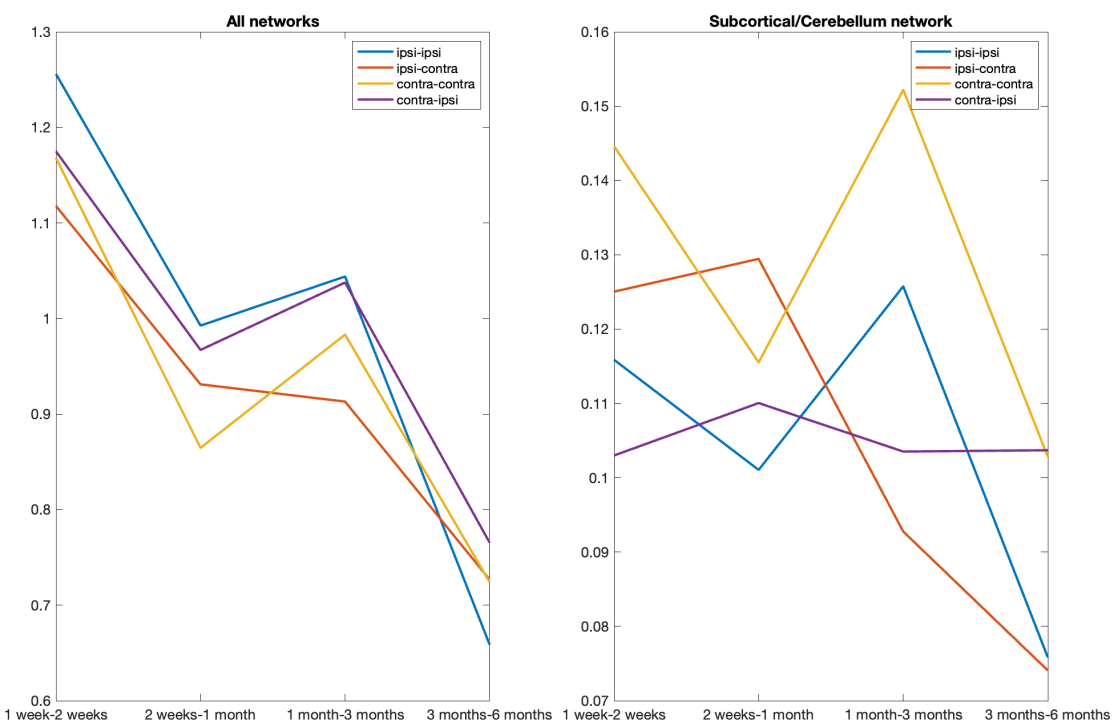


Figure A.6: Number of remaps in

Left: Number of remaps over 4 time point intervals split into whether the source and target network were in the contralesional or ipsilesional hemisphere. Left: number of remaps organized by hemisphere in only the subcortical/cerebellum network.

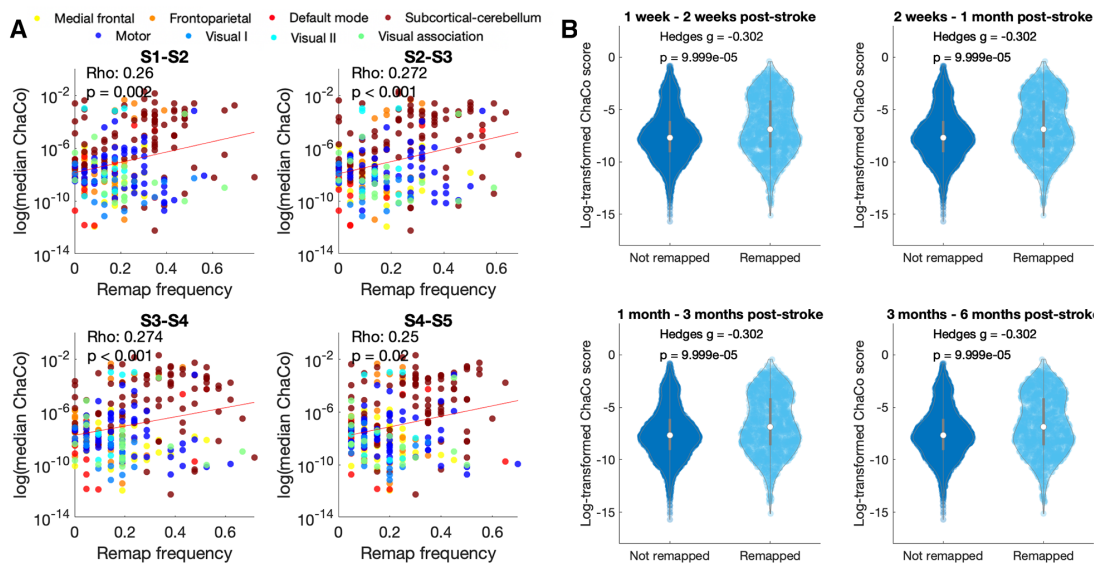


Figure A.7: Functional network visualizations.

8 functional networks identified by (Finn et al. 2015) by clustering healthy functional connectivity matrices.

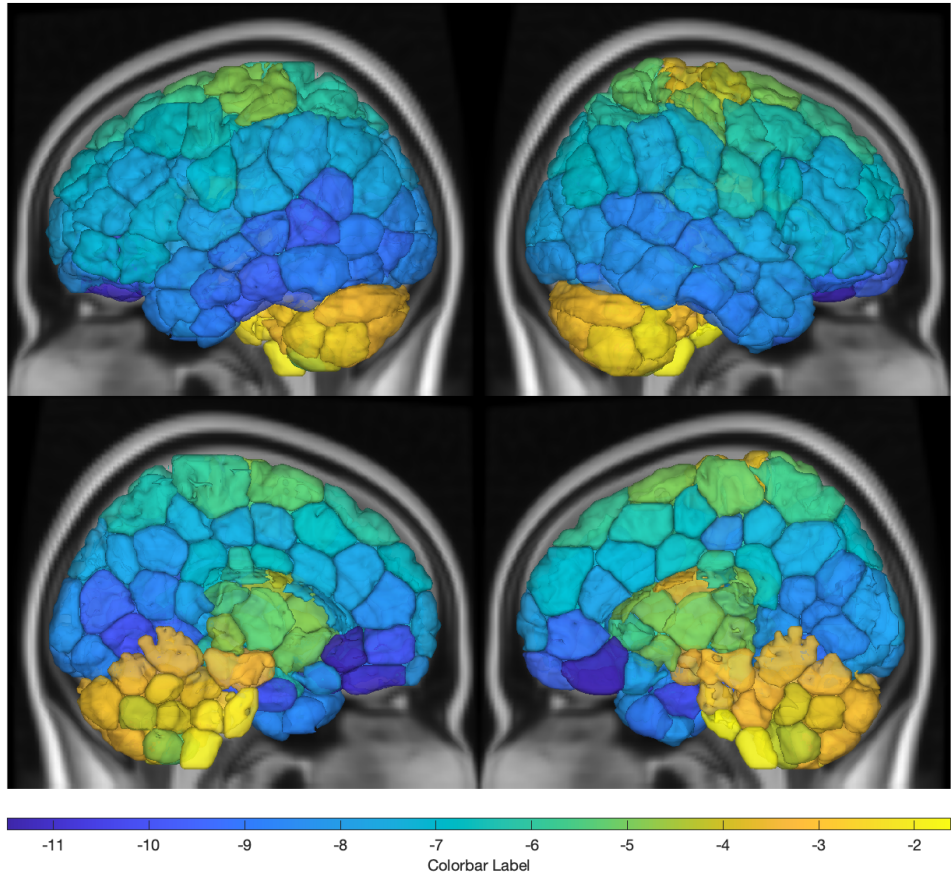


Figure A.8: Functional network visualizations.

8 functional networks identified by (Finn et al. 2015) by clustering healthy functional connectivity matrices.

BIBLIOGRAPHY

- Duncan, P W, S M Lai, and J Keighley. 2000. "Defining post-stroke recovery: implications for design and interpretation of drug trials" [inlangen]. *Neuropharmacology* 39, no. 5 (): 835–841.
- Grefkes, Christian, et al. 2008. "Cortical connectivity after subcortical stroke assessed with functional magnetic resonance imaging" [inlangen]. *Ann. Neurol.* 63, no. 2 (): 236–246.
- Rehme, Anne K, and Christian Grefkes. 2013. "Cerebral network disorders after stroke: evidence from imaging-based connectivity analyses of active and resting brain states in humans" [inlangen]. *J. Physiol.* 591, no. 1 (): 17–31.
- Winship, Ian R, and Timothy H Murphy. 2009. "Remapping the somatosensory cortex after stroke: insight from imaging the synapse to network" [inlangen]. *Neuroscientist* 15, no. 5 (): 507–524.
- Adam, Ramina, et al. 2020. "Functional reorganization during the recovery of contralesional target selection deficits after prefrontal cortex lesions in macaque monkeys" [inlangen]. *Neuroimage* 207 (): 116339.
- Murata, Yumi, et al. 2015. "Temporal plasticity involved in recovery from manual dexterity deficit after motor cortex lesion in macaque monkeys" [inlangen]. *J. Neurosci.* 35, no. 1 (): 84–95.
- Brown, Craig E, et al. 2009. "In vivo voltage-sensitive dye imaging in adult mice reveals that somatosensory maps lost to stroke are replaced over weeks by new structural and functional circuits with prolonged modes of activation within both the peri-infarct zone and distant sites" [inlangen]. *J. Neurosci.* 29, no. 6 (): 1719–1734.

- Ward, N S, et al. 2003. "Neural correlates of motor recovery after stroke: a longitudinal fMRI study" [inlangen]. *Brain* 126, no. Pt 11 (): 2476–2496.
- Park, Chang-Hyun, et al. 2011. "Longitudinal changes of resting-state functional connectivity during motor recovery after stroke" [inlangen]. *Stroke* 42, no. 5 (): 1357–1362.
- Lu, Jie, et al. 2011. "Focal pontine lesions provide evidence that intrinsic functional connectivity reflects polysynaptic anatomical pathways" [inlangen]. *J. Neurosci.* 31, no. 42 (): 15065–15071.
- Saia, V, and L Pantoni. 2009. "Progressive stroke in pontine infarction" [inlangen]. *Acta Neurol. Scand.* 120, no. 4 (): 213–215.
- Carrera, Emmanuel, and Giulio Tononi. 2014. "Diaschisis: past, present, future" [inlangen]. *Brain* 137, no. Pt 9 (): 2408–2422.
- Griffis, Joseph C, et al. 2020. "Damage to the shortest structural paths between brain regions is associated with disruptions of resting-state functional connectivity after stroke" [inlangen]. *Neuroimage* 210 (): 116589.
- Conte, Donatello, et al. 2004. "Thirty Years Of Graph Matching In Pattern Recognition". *Int. J. Pattern Recognit Artif Intell.* 18, no. 3 (): 265–298.
- Osmanlıoğlu, Yusuf, et al. 2019. "System-level matching of structural and functional connectomes in the human brain" [inlangen]. *Neuroimage* 199 (): 93–104.
- Whitfield-Gabrieli, Susan, and Alfonso Nieto-Castanon. 2012. "Conn: a functional connectivity toolbox for correlated and anticorrelated brain networks" [inlangen]. *Brain Connect.* 2, no. 3 (): 125–141.

- Behzadi, Yashar, et al. 2007. "A component based noise correction method (CompCor) for BOLD and perfusion based fMRI" [inlangen]. *Neuroimage* 37, no. 1 (): 90–101.
- Power, Jonathan D, et al. 2012a. "Spurious but systematic correlations in functional connectivity MRI networks arise from subject motion" [inlangen]. *Neuroimage* 59, no. 3 (): 2142–2154.
- Shen, X, et al. 2013. "Groupwise whole-brain parcellation from resting-state fMRI data for network node identification" [inlangen]. *Neuroimage* 82 (): 403–415.
- Finn, Emily S, et al. 2015. "Functional connectome fingerprinting: identifying individuals using patterns of brain connectivity" [inlangen]. *Nat. Neurosci.* 18, no. 11 (): 1664–1671.
- Wodeyar, Anirudh, et al. 2020. "Damage to the structural connectome reflected in resting-state fMRI functional connectivity". *Network Neuroscience* (): 1–22.
- Liégeois, Raphaël, et al. 2020. "Revisiting correlation-based functional connectivity and its relationship with structural connectivity". *Network Neuroscience* (): 1–17.
- Golub, Gene H, Per Christian Hansen, and Dianne P O'Leary. 1999. "Tikhonov Regularization and Total Least Squares". *SIAM J. Matrix Anal. Appl.* 21, no. 1 (): 185–194.
- Hillis, A E, et al. 2002. "Subcortical aphasia and neglect in acute stroke: the role of cortical hypoperfusion" [inlangen]. *Brain* 125, no. Pt 5 (): 1094–1104.
- Corbetta, Maurizio, et al. 2015. "Common behavioral clusters and subcortical anatomy in stroke" [inlangen]. *Neuron* 85, no. 5 (): 927–941.

- Duering, Marco, et al. 2015. "Acute infarcts cause focal thinning in remote cortex via degeneration of connecting fiber tracts" [inlangen]. *Neurology* 84, no. 16 (): 1685–1692.
- Cheng, Bastian, et al. 2015. "Structural plasticity of remote cortical brain regions is determined by connectivity to the primary lesion in subcortical stroke" [inlangen]. *J. Cereb. Blood Flow Metab.* 35, no. 9 (): 1507–1514.
- Kuceyeski, Amy, et al. 2013. "The Network Modification (NeMo) Tool: elucidating the effect of white matter integrity changes on cortical and subcortical structural connectivity" [inlangen]. *Brain Connect.* 3 (5): 451–463.
- Osmanlioğlu, Yusuf, et al. 2020. "Connectomic consistency: a systematic stability analysis of structural and functional connectivity" [inlangen]. *J. Neural Eng.* 17, no. 4 (): 045004.
- Murphy, Timothy H, and Dale Corbett. 2009. "Plasticity during stroke recovery: from synapse to behaviour" [inlangen]. *Nat. Rev. Neurosci.* 10, no. 12 (): 861–872.
- Lee, Kyoung Bo, et al. 2015. "Six-month functional recovery of stroke patients: a multi-time-point study" [inlangen]. *Int. J. Rehabil. Res.* 38, no. 2 (): 173–180.
- Kuceyeski, Amy F, et al. 2019. "Longitudinal increases in structural connectome segregation and functional connectome integration are associated with better recovery after mild TBI" [inlangen]. *Hum. Brain Mapp.* 40, no. 15 (): 4441–4456.
- Honey, C J, et al. 2009. "Predicting human resting-state functional connectivity from structural connectivity" [inlangen]. *Proc. Natl. Acad. Sci. U. S. A.* 106, no. 6 (): 2035–2040.
- Guggisberg, Adrian G, et al. 2019. "Brain networks and their relevance for stroke rehabilitation" [inlangen]. *Clin. Neurophysiol.* 130, no. 7 (): 1098–1124.

- Griffis, Joseph C, et al. 2019. "Structural Disconnections Explain Brain Network Dysfunction after Stroke" [inlangen]. *Cell Rep.* 28, no. 10 (): 2527–2540.e9.
- Mottolese, Carmine, et al. 2013. "Mapping motor representations in the human cerebellum" [inlangen]. *Brain* 136, no. Pt 1 (): 330–342.
- Zhang, Ye, et al. 2016. "Relationship between functional connectivity and motor function assessment in stroke patients with hemiplegia: a resting-state functional MRI study" [inlangen]. *Neuroradiology* 58, no. 5 (): 503–511.
- Yourganov, Grigori, et al. 2021. "Effect of stroke on contralateral functional connectivity" [inlangen]. *Brain Connect.* ()�.
- Krakauer, J W, and R S Marshall. 2015. "The proportional recovery rule for stroke revisited" [inlangen]. *Ann. Neurol.* 78, no. 6 (): 845–847.
- Braun, Urs, et al. 2021. "Brain network dynamics during working memory are modulated by dopamine and diminished in schizophrenia" [inlangen]. *Nat. Commun.* 12, no. 1 (): 3478.
- Adhikari, Mohit H, et al. 2020. "Resting-State Co-activation Patterns as Promising Candidates for Prediction of Alzheimer's Disease in Aged Mice" [inlangen]. *Front. Neural Circuits* 14:612529.
- Kaiser, Roselinde H, et al. 2019. "Abnormal frontoinsular-default network dynamics in adolescent depression and rumination: a preliminary resting-state co-activation pattern analysis" [inlangen]. *Neuropsychopharmacology* 44, no. 9 (): 1604–1612.
- Cornblath, Eli J, et al. 2020. "Temporal sequences of brain activity at rest are constrained by white matter structure and modulated by cognitive demands" [inlangen]. *Commun Biol* 3, no. 1 (): 261.

- Savva, Antonis D, Georgios D Mitsis, and George K Matsopoulos. 2019. "Assessment of dynamic functional connectivity in resting-state fMRI using the sliding window technique" [inlangen]. *Brain Behav.* 9, no. 4 (): e01255.
- Bonkhoff, Anna K, et al. 2020a. "Acute ischaemic stroke alters the brain's preference for distinct dynamic connectivity states" [inlangen]. *Brain* 143, no. 5 (): 1525–1540.
- Bonkhoff, Anna K, et al. 2020b. "Dynamic functional connectivity analysis reveals transiently increased segregation in patients with severe stroke".
- Zamani Esfahlani, Farnaz, et al. 2020. "High-amplitude cofluctuations in cortical activity drive functional connectivity" [inlangen]. *Proc. Natl. Acad. Sci. U. S. A.* 117, no. 45 (): 28393–28401.
- Betzel, Richard F, et al. 2021. "Individualized event structure drives individual differences in whole-brain functional connectivity" [inlangen].
- Baker, Adam P, et al. 2014. "Fast transient networks in spontaneous human brain activity" [inlangen]. *Elife* 3 (): e01867.
- Tscherpel, Caroline, et al. 2020. "The differential roles of contralesional frontoparietal areas in cortical reorganization after stroke" [inlangen]. *Brain Stimul.* 13, no. 3 (): 614–624.
- Hensel, Lukas, et al. 2022. "Recovered grasping performance after stroke depends on interhemispheric frontoparietal connectivity" [inlangen]. *Brain* ().
- Hordacre, Brenton, et al. 2021. "Fronto-parietal involvement in chronic stroke motor performance when corticospinal tract integrity is compromised" [inlangen]. *Neuroimage Clin* 29 (): 102558.

- Fugl-Meyer, A R, et al. 1975. "The post-stroke hemiplegic patient. 1. a method for evaluation of physical performance" [inlangen]. *Scand. J. Rehabil. Med.* 7 (1): 13–31.
- Olafson, Emily R, et al. 2021. "Functional connectome reorganization relates to post-stroke motor recovery and structural and functional disconnection" [inlangen]. *Neuroimage* 245 (): 118642.
- Avants, Brian B, et al. 2011. "A reproducible evaluation of ANTs similarity metric performance in brain image registration" [inlangen]. *Neuroimage* 54, no. 3 (): 2033–2044.
- Power, Jonathan D, et al. 2012b. "Spurious but systematic correlations in functional connectivity MRI networks arise from subject motion". *Neuroimage*.
- Desikan, Rahul S, et al. 2006. "An automated labeling system for subdividing the human cerebral cortex on MRI scans into gyral based regions of interest" [inlangen]. *Neuroimage* 31, no. 3 (): 968–980.
- Craddock, R Cameron, et al. 2012. "A whole brain fMRI atlas generated via spatially constrained spectral clustering" [inlangen]. *Hum. Brain Mapp.* 33, no. 8 (): 1914–1928.
- Benjamini, Yoav, and Yosef Hochberg. 1995. "Controlling the False Discovery Rate: A Practical and Powerful Approach to Multiple Testing". *J. R. Stat. Soc. Series B Stat. Methodol.* 57 (1): 289–300.
- Tang, Yuchun, et al. 2018. "A probabilistic atlas of human brainstem pathways based on connectome imaging data" [inlangen]. *Neuroimage* 169 (): 227–239.
- De Leener, Benjamin, et al. 2017. "SCT: Spinal Cord Toolbox, an open-source software for processing spinal cord MRI data" [inlangen]. *Neuroimage* 145, no. Pt A (): 24–43.

Kundert, Robinson, et al. 2019. "What the Proportional Recovery Rule Is (and Is Not): Methodological and Statistical Considerations". *Neurorehabil. Neural Repair* 33, no. 11 (): 876–887.

Hope, Thomas M H, et al. 2019. "Recovery after stroke: not so proportional after all?" [inlangen]. *Brain* 142, no. 1 (): 15–22.

Olafson, Emily. 2022. *Brain activity states in pontine stroke*.

Katan, Mira, and Andreas Luft. 2018. "Global Burden of Stroke" [inlangen]. *Semin. Neurol.* 38, no. 2 (): 208–211.

Kelly-Hayes, Margaret, et al. 2003. "The influence of gender and age on disability following ischemic stroke: the Framingham study" [inlangen]. *J. Stroke Cerebrovasc. Dis.* 12 (3): 119–126.

Bonkhoff, Anna K, and Christian Grefkes. 2022. "Precision medicine in stroke: towards personalized outcome predictions using artificial intelligence" [inlangen]. *Brain* 145, no. 2 (): 457–475.

Boyd, Lara A, et al. 2017. "Biomarkers of stroke recovery: Consensus-based core recommendations from the Stroke Recovery and Rehabilitation Roundtable" [inlangen]. *Int. J. Stroke* 12, no. 5 (): 480–493.

Tozlu, Ceren, et al. 2020. "Machine Learning Methods Predict Individual Upper-Limb Motor Impairment Following Therapy in Chronic Stroke" [inlangen]. *Neurorehabil. Neural Repair* 34, no. 5 (): 428–439.

Kuceyeski, Amy, et al. 2016. "Structural connectome disruption at baseline predicts 6-months post-stroke outcome" [inlangen]. *Hum. Brain Mapp.* 37, no. 7 (): 2587–2601.

Salvalaggio, Alessandro, et al. 2020. "Post-stroke deficit prediction from lesion and indirect structural and functional disconnection" [inlangen]. *Brain* ().

- Bowren, Mark, et al. 2022. "Post-stroke outcomes predicted from multivariate lesion-behaviour and lesion network mapping" [inlangen]. *Brain* ().
- Zhu, Lin L, et al. 2010. "Lesion load of the corticospinal tract predicts motor impairment in chronic stroke" [inlangen]. *Stroke* 41, no. 5 (): 910–915.
- Feng, Wuwei, et al. 2015. "Corticospinal tract lesion load: An imaging biomarker for stroke motor outcomes" [inlangen]. *Ann. Neurol.* 78, no. 6 (): 860–870.
- Findlater, Sonja E, et al. 2019. "Comparing CST Lesion Metrics as Biomarkers for Recovery of Motor and Proprioceptive Impairments After Stroke" [inlangen]. *Neurorehabil. Neural Repair* 33, no. 10 (): 848–861.
- Lam, Timothy K, et al. 2018. "Variability in stroke motor outcome is explained by structural and functional integrity of the motor system" [inlangen]. *Sci. Rep.* 8, no. 1 (): 9480.
- Pineiro, R, et al. 2000. "Relating MRI changes to motor deficit after ischemic stroke by segmentation of functional motor pathways" [inlangen]. *Stroke* 31, no. 3 (): 672–679.
- Kim, Bokkyu, and Carolee Winstein. 2017. "Can Neurological Biomarkers of Brain Impairment Be Used to Predict Poststroke Motor Recovery? A Systematic Review" [inlangen]. *Neurorehabil. Neural Repair* 31, no. 1 (): 3–24.
- Park, Chang-Hyun, Nancy Kou, and Nick S Ward. 2016. "The contribution of lesion location to upper limb deficit after stroke" [inlangen]. *J. Neurol. Neurosurg. Psychiatry* 87, no. 12 (): 1283–1286.
- Ito, Kaori L, et al. 2022. "Corticospinal Tract Lesion Load Originating From Both Ventral Premotor and Primary Motor Cortices Are Associated With Post-stroke Motor Severity" [inlangen]. *Neurorehabil. Neural Repair* 36, no. 3 (): 179–182.

- Rondina, Jane M, et al. 2016. "Decoding post-stroke motor function from structural brain imaging" [inlangen]. *Neuroimage Clin* 12 (): 372–380.
- Rondina, Jane M, Chang-Hyun Park, and Nick S Ward. 2017. "Brain regions important for recovery after severe post-stroke upper limb paresis" [inlangen]. *J. Neurol. Neurosurg. Psychiatry* 88, no. 9 (): 737–743.
- Schulz, Robert, et al. 2012. "Assessing the integrity of corticospinal pathways from primary and secondary cortical motor areas after stroke" [inlangen]. *Stroke* 43, no. 8 (): 2248–2251.
- Mah, Yee-Haur, et al. 2014. "Human brain lesion-deficit inference remapped" [inlangen]. *Brain* 137, no. Pt 9 (): 2522–2531.
- Bzdok, Danilo, Denis Engemann, and Bertrand Thirion. 2020. "Inference and Prediction Diverge in Biomedicine" [inlangen]. *Patterns (N Y)* 1, no. 8 (): 100119.
- Bates, Elizabeth, et al. 2003. "Voxel-based lesion-symptom mapping" [inlangen]. *Nat. Neurosci.* 6, no. 5 (): 448–450.
- Karnath, Hans-Otto, et al. 2020. "Lesion-Behavior Mapping in Cognitive Neuroscience: A Practical Guide to Univariate and Multivariate Approaches". In *Spatial Learning and Attention Guidance*, ed. by Stefan Pollmann, 209–238. New York, NY: Springer US.
- Ivanova, Maria V, et al. 2021. "An empirical comparison of univariate versus multivariate methods for the analysis of brain-behavior mapping" [inlangen]. *Hum. Brain Mapp.* 42, no. 4 (): 1070–1101.
- Zhang, Yongsheng, et al. 2014. "Multivariate lesion-symptom mapping using support vector regression" [inlangen]. *Hum. Brain Mapp.* 35, no. 12 (): 5861–5876.

- Sperber, Christoph, Daniel Wiesen, and Hans-Otto Karnath. 2019. “An empirical evaluation of multivariate lesion behaviour mapping using support vector regression” [inlangen]. *Hum. Brain Mapp.* 40, no. 5 (): 1381–1390.
- Sperber, Christoph, Joseph Griffis, and Vanessa Kasties. 2022. “Indirect structural disconnection-symptom mapping” [inlangen]. *Brain Struct. Funct.* ().
- Sperber, Christoph. 2020. “Rethinking causality and data complexity in brain lesion-behaviour inference and its implications for lesion-behaviour modelling” [inlangen]. *Cortex* 126 (): 49–62.
- Kimberg, Daniel Y, H Branch Coslett, and Myrna F Schwartz. 2007. “Power in VPower in voxel-based lesion–symptoxel-based lesion–symptom mapping om mapping”.
- Rorden, Chris, Julius Fridriksson, and Hans-Otto Karnath. 2009. “An evaluation of traditional and novel tools for lesion behavior mapping” [inlangen]. *Neuroimage* 44, no. 4 (): 1355–1362.
- Kasties, Vanessa, Hans-Otto Karnath, and Christoph Sperber. 2021. “Strategies for feature extraction from structural brain imaging in lesion-deficit modelling” [inlangen]. *Hum. Brain Mapp.* 42, no. 16 (): 5409–5422.
- Liew, Sook-Lei, et al. 2020. “The ENIGMA Stroke Recovery Working Group: Big data neuroimaging to study brain-behavior relationships after stroke” [inlangen]. *Hum. Brain Mapp.* ().
- Gladstone, David J, Cynthia J Danells, and Sandra E Black. 2002. “The fugl-meyer assessment of motor recovery after stroke: a critical review of its measurement properties” [inlangen]. *Neurorehabil. Neural Repair* 16, no. 3 (): 232–240.

- Yozbatiran, Nuray, Lucy Der-Yeghaian, and Steven C Cramer. 2008. "A standardized approach to performing the action research arm test" [inlangen]. *Neurorehabil. Neural Repair* 22 (1): 78–90.
- Sulter, G, C Steen, and J De Keyser. 1999. "Use of the Barthel index and modified Rankin scale in acute stroke trials" [inlangen]. *Stroke* 30, no. 8 (): 1538–1541.
- Lyden, Patrick. 2017. "Using the National Institutes of Health Stroke Scale: A Cautionary Tale" [inlangen]. *Stroke* 48, no. 2 (): 513–519.
- Bernhardt, Julie, et al. 2017. "Agreed definitions and a shared vision for new standards in stroke recovery research: The Stroke Recovery and Rehabilitation Roundtable taskforce" [inlangen]. *Int. J. Stroke* 12, no. 5 (): 444–450.
- Stinear, Cathy M. 2017. "Prediction of motor recovery after stroke: advances in biomarkers" [inlangen]. *Lancet Neurol.* 16, no. 10 (): 826–836.
- Archer, Derek B, David E Vaillancourt, and Stephen A Coombes. 2018. "A Template and Probabilistic Atlas of the Human Sensorimotor Tracts using Diffusion MRI" [inlangen]. *Cereb. Cortex* 28, no. 5 (): 1685–1699.
- Pustina, Dorian, et al. 2018. "Improved accuracy of lesion to symptom mapping with multivariate sparse canonical correlations" [inlangen]. *Neuropsychologia* 115 (): 154–166.
- Smith, Robert E, et al. 2015. "SIFT2: Enabling dense quantitative assessment of brain white matter connectivity using streamlines tractography" [inlangen]. *Neuroimage* 119 (): 338–351.
- Fischl, Bruce, et al. 2002. "Whole brain segmentation: automated labeling of neuroanatomical structures in the human brain" [inlangen]. *Neuron* 33, no. 3 (): 341–355.

- Guyon, Isabelle, and Andre Elisseeff. 2003. "An introduction to variable and feature selection". *J. Mach. Learn. Res.* 3:1157–1182.
- Hall, Mark A. 1999. *Correlation-based Feature Selection for Machine Learning*. <https://www.cs.waikato.ac.nz/~mhall/thesis.pdf>. Accessed: 2022-12-24.
- Pudjihartono, Nicholas, et al. 2022. "A Review of Feature Selection Methods for Machine Learning-Based Disease Risk Prediction" [inlangen]. *Front Bioinform* 2 (): 927312.
- Hastie, Trevor, Jerome Friedman, and Robert Tibshirani. 2001. *The Elements of Statistical Learning*. Springer New York.